Article

Not peer-reviewed version

Comparative Pore-Connectivity and Wettability Characteristics of the Fresh-Water and Saline Lacustrine Tuffaceous Shales: Triggering Mechanisms and Multi-Scale Models for Differential Reservoir-Forming Patterns

Wei Yang *

Posted Date: 8 December 2023

doi: 10.20944/preprints202312.0616.v1

Keywords: tuffaceous shale; devitrification; wettability; pore connectivity; Yanchang Formation; Jingjingzigou Formation

Article

Comparative Pore-Connectivity and Wettability Characteristics of the Fresh-Water and Saline Lacustrine Tuffaceous Shales: Triggering Mechanisms and Multi-Scale Models for Differential Reservoir-Forming Patterns

Wei Yang [a,b,c,*], Baojian Shen [a,d,*], Mou Ding [b,c], Rui Zhao [a,e], Zilong Zhang [b,c], Zhiming Li [a,d], Hanwen Hu [a,d], Fan Feng [a,d] and Ming Xie [b,c]

[a] State Key Laboratory of Shale Oil and Gas Enrichment Mechanisms and Effective Development, Beijing, 100083, China
[b] National Key Laboratory of Petroleum Resources and Engineering, China University of Petroleum (Beijing), Beijing, China. 102249
[c] Unconventional Oil and Gas Research Institute, China University of Petroleum, Beijing, 102249, China
[d] Sinopec Petroleum Exploration and Production Research Institute, Beijing 100083, China
[e] China Petroleum & Chemical Corporation, Beijing 100728, China
* Correspondence: yangw@pku.edu.cn (W.Y.), Tel.: +86-10-89739051; fax: +86-10-89739051; shenbaoj@163.com (B.S.)

Abstract: The continental shale layers are more complex in matrix pore-microfracture interactions and connectivity characteristics under the influence of tuff devitrification, which limits the explicit understanding of the coupling relationship between wettability and pore structure, as well as hydrocarbon flow behavior. Therefore, the influence of tuffaceous components on the reservoir formation mechanism and oil-rich effect of the continental shale formation system is a critical issue to be solved. The Upper Triassic Yanchang Formation tuffaceous shale in Ordos Basin and the Middle Permian Jingjingzigou Formation tuffaceous shale in the southern margin of Junggar Basin is taken as the research objects, using whole-rock mineral composition analysis, FE-SEM observation and digital image processing and extraction, as well as wettability angle determination and spontaneous imbibition experiments to illustrate the influence of the difference of devitrification extent on reservoir pore connectivity and interfacial wettability in two different environments of freshwater and saline lacustrine basins, and summarize the reservoir formation differential pattern under the influence of devitrification. The results show that the saline lacustrine is significantly modified by devitrification. The pore plane porosity of the devitrified tuffaceous shales in the saline lacustrine is higher than that of the tuffaceous shales in the freshwater; the oleophilic of the saline lacustrine tuffaceous shales is better than that of the tuffaceous shales in the freshwater, moreover, the pore connectivity of the saline lacustrine tuffaceous shales is better than that of the tuffaceous shales in the freshwater. Wettability and connectivity control the storage performance of shale oil in the tuffaceous shales formation system. The more oleophilic the reservoir wettability is, the better the pore connectivity is, and the better the reservoir of tuffaceous shale formation system is. According to the different extents of devitrification, two different reservoir formation models of freshwater and saline lacustrine are established, which are of great theoretical and practical significance to enrich the theory of shale oil enrichment and reservoir formation in the continental shale formation system and to guide the exploration of continental shale oil benefits.

Keywords: tuffaceous shale; devitrification; wettability; pore connectivity; Yanchang Formation; Jingjingzigou Formation

1. Introduction

Tuffaceous reservoirs, which are closely related to volcanic activity, have become one of the current research hotspots in the field of earth sciences [1,2]. Volcanic activity is instantaneous and

 doi:10.20944/preprints202312.0616.v1

isochronous, and the volcanic ash erupted during volcanic activity is also instantaneous and isochronous during deposition, so volcanic ash is widely distributed in various sedimentary basins with distinctive characteristics [3]. Volcanic ash is rich in nutrients, such as, Fe, P, and Ca, which are capable of promoting algae blooms and resulting in high-quality hydrocarbon source rocks in lake basins [4−6]. Tuffs can also be used to reconstruct surrounding tectonic magmatic geological events [7−9], as well as to clarify the timing and sequence of development of geological events and to restore paleoenvironments [10]. In addition, tuffs can be used as oil and gas reservoirs, and tuff-bearing reservoirs usually have favorable hydrocarbon shows, and high industrial gas flows and industrial oil flows can be seen in tuff-bearing reservoirs in some developed areas, such as the Akita and Niigata basins in Japan [11], the Richland field in the United States [12], the Neuquén Basin in Argentina [13], the Junggar Basin in China [14] and the Ordos Basin [15], among others. In recent years, the research on tuffs or tuff-bearing reservoirs has become a hot topic, mainly focusing on their lithological characteristics, reservoir spatial types and features, and physical properties [16−18]. In the exploration and development of unconventional oil and gas, tuffs or tuffaceous shales generally have better pore space and imbibition capacity [19,20], and these tuffs or tuffaceous reservoirs with superior reservoir conditions are mainly affected by devitrification, and the reservoir is more favorable for hydrocarbon enrichment after devitrification [18].

Devitrification is the process that vitreous silica in volcanic ash gradually shifts to crystalline state. And in the process of shifting to the crystalline state, the new minerals formed by the devitrified process are reduced in volume, so that a large number of microporosity can be formed between different mineral particles; the new minerals formed by devitrified will be dissolved under the action of fluids and produce dissolved porosity, therefore, the porosity in the reservoir can be effectively enhanced after devitrified [21]. Wettability, as one of the important surface properties of an object, is mainly used to reflect the tendency between solids and liquids. It is shown that wettability affects the effect of the interaction between geological fluids and reservoirs [22,23]. The difference of wettability directly affects the reservoir storage capacity. The contact angle method can measure the wettability of rocks most intuitively and effectively, and fluid flow dispersion on the rock surface can be observed. Spontaneous imbibition is the process by which a wettable fluid in the pores of a rock spontaneously replaces another non-wettable fluid by capillary forces. Through spontaneous imbibition experiments, we are able to obtain the influencing factors of the storage capacity inside the rock, such as, wettability, pore structure, viscosity, and interfacial tension [24−27]. When the tuffaceous components in the reservoir are devitrification, the special pore structure of the devitrification pores (small size, small pore throat, low pore-throat ratio) leads to similar capillary forces, which facilitates hydrocarbon retention and also contributes to the wettability inversion at the interface of the mixed tuffaceous shales [28−30]. Identifying the internal pore characteristics of the reservoir and the wettability between the reserve and the fluid enables us to understand the imbibition pattern of the fluid in the reservoir and facilitates the development of the reservoir in the reservoir.

However, devitrified pores, as the most important reservoir space in tuffs and tuffaceous reservoirs, lack specific discussions and comparative studies on the differences in the degree of devitrification, and the controlling effects of devitrification differences on reservoir wettability and pore connectivity remain unclear.

For the purpose of researching the difference of tuff devitrification in different environments and the difference of devitrification on the improvement of reservoir wettability and pore connectivity, the Upper Triassic Yanchang Formation in the Ordos Basin and the Middle Permian Jingjingzigou Formation in the Junggar Basin are selected as samples and analyzed by field emission scanning electron microscope observation, Image Pro Plus software image processing, contact angle experiments and spontaneous imbibition experiments. Using observation methods at different scales, the observed pores are described in detail and combined with image processing software to quantitatively analyze many types of devitrified causal pores. By determining the wettability angle and the relative wettability parameters, the wettability of various types of devitrified samples can be identified. To study the transport capacity of organic fluids in devitrified oil-bearing reservoirs

 doi:10.20944/preprints202312.0616.v1

through spontaneous imbibition experiments can evaluate the pore connectivity of the reservoirs after devitrification. Finally, using the above experimental results to establish the difference patterns of devitrification in different environments, as well as to portray the difference patterns of wettability and pore connectivity within the reservoir after devitrification in different environments. Through the above research, it provides new research directions and perspectives for future unconventional oil and gas exploration and development and has a significant theoretical and realistic significance in guidance of terrestrial oil and gas exploration and development.

2. Geological Setting

The Ordos Basin is the second largest sedimentary basin in China, spanning Shaanxi, Gansu, Ningxia, Shanxi and Inner Mongolia (Figure 1a). The Ordos Basin is tectonically located in the southwestern part of the North China Craton, which is a large multi-rotational Craton basin with stable overall lift, depressional migration, and simple tectonics [31], and the basin structure is relatively simple and can be divided into six tectonic units (Figure 1b): the Yimeng uplift in the north, the Weibei uplift in the south, the Western margin thrust belt and the Tianhuan depression in the west, the Jinxi fault-fold belt in the east, and the Yishan slope in the center [32,33]. The Ordos Basin was formed in the Cambrian period at the beginning and it has been subjected to superposition of multiple tectonic movements to form the current tectonic pattern [34]. The Ordos Basin is rich in oil and gas resources, and the Triassic Yanchang Formation is widely distributed in the basin as the most abundant formation in oil and gas resources. The Yanchang Formation sedimentary period began at the end of the Middle Triassic, when the Ordos Basin changed from marine sedimentation to terrestrial lake sedimentation. Under the influence of tectonic movements, the basin was formed a large inland freshwater lake basin with large area and wide waters, as well as a set of terrestrial clastic rock system characterized by fluvial-lacustrine facies [35,36]. The Yanchang Formation is subdivided into 10 substrata (Figure 1c) according to its depositional environment and lithologic combination variations. During the deposition of the Yanchang Formation, the lake basin regressed and expanded significantly due to strong tectonic movements with continuous eruptions of volcanic ash from surrounding volcanic movements spilling into the lake basin. A large number of organic-rich shales and tuffs were deposited under semi-deep to deep lake conditions, and tuffs were able to be widely distributed in the Yanchang Formation [37–40]. Within the Yanchang Formation, a thick layer of organic-rich shale is mixed with tuff layers where the thickness of individual tuff layers varies from a few millimeters to tens of centimeters, and the accumulated thickness can reach several meters [41–42].

Preprints (www.preprints.org) | NOT PEER-REVIEWED | Posted: 8 December 2023 doi:10.20944/preprints202312.0616.v1

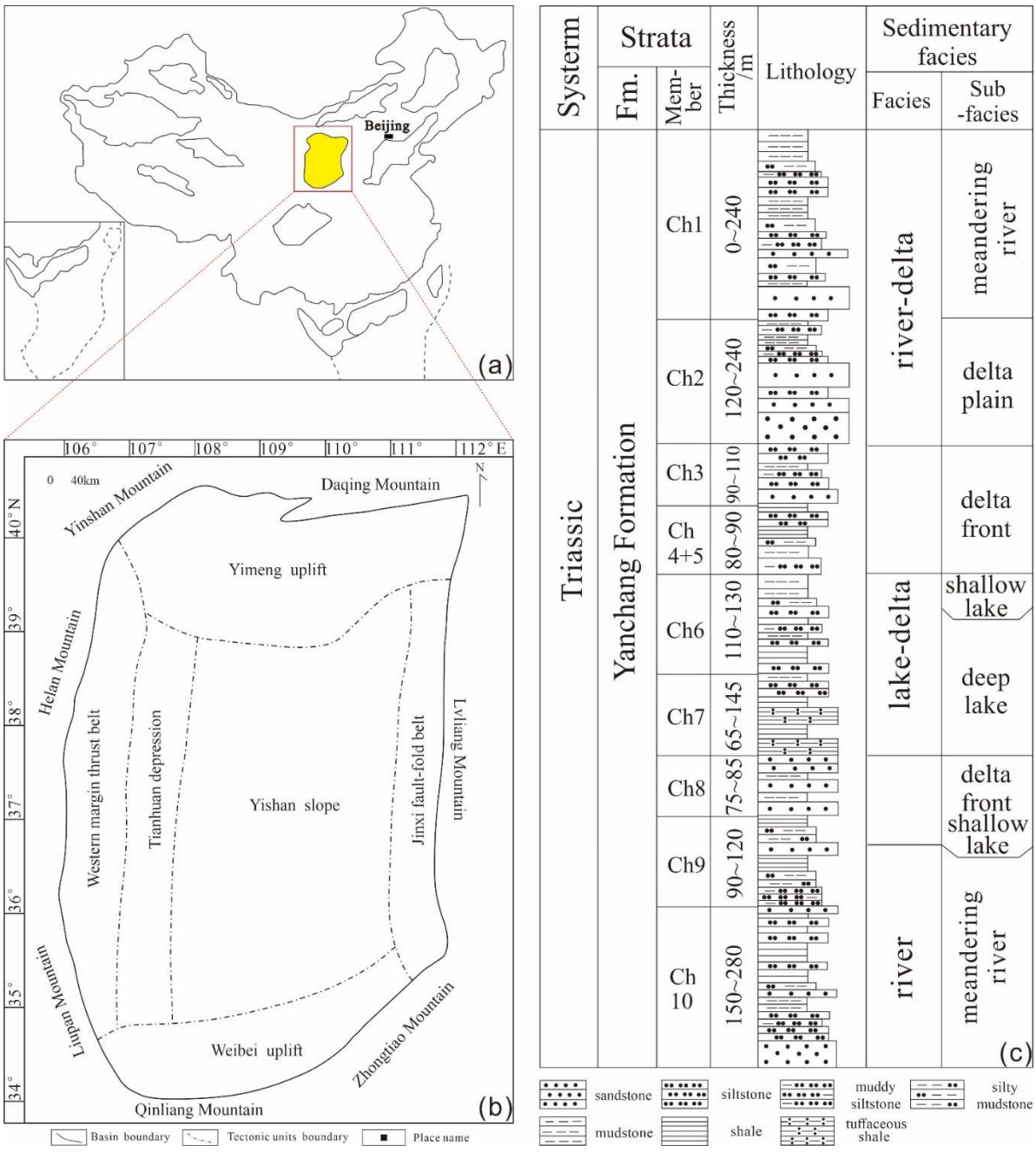

Figure 1. (a) Geographic location of the Ordos Basin in China; (b) Geological background of the Ordos Basin, as well as the study area and well locations; (c) Stratigraphy, thickness, lithology, and sedimentary phases of the Upper Triassic Yanchang Formation in the Ordos Basin.

The Junggar Basin is located in the northern part of the Xinjiang Province with a general isosceles triangle shape (Figure 2a), which is characterized by a narrow southern width in the north and a slope from east to west [43]. The Junggar Basin has undergone multiple periods of tectonic deformation and superimposed transformation, including the Hercynian period, Indochina period, Yanshan period and Himalayan periods, at the same time alternating extension, extrusion, shearing and other tectonic effects, making the region tectonically complex, with strong stratigraphic folding and the formation of a large number of unequal or isoclinal folds [44]. Therefore, the Junggar Basin can be divided into six secondary tectonic units (Figure 2b), including the Ulungu depression and the Lvliang uplift in the north, the Central depression in the abdomen, the Western uplift, the Eastern uplift, and the Tianshan Mountain thrust belt in the south [45,46]. The Middle Permian Jingjingzigou Formation is mainly developed near the foothills of the Bogda Mountains on the southern margin of

Preprints (www.preprints.org) | NOT PEER-REVIEWED | Posted: 8 December 2023 doi:10.20944/preprints202312.0616.v1

the Junggar Basin (Figure 2c), in integrated contact with the underlying Ulapo Formation, with continuous transition to the overlying Lucaogou Formation [47]. During the Middle Permian, the warm humid climate changed to dry and hot seasonal climate, thus the terrestrial sedimentation of some river-delta-lake facies in the southern edge of Junggar Basin was affected by the climate change, resulting in the overall shallowing of the water system and the increasing salinity of the water system to form a sedimentary environment dominated by saline lake basin background [48]. In this tectonic-sedimentary context, the Middle Permian Jingjingzigou Formation is characterized by the widespread development of tuffs or tuffaceous intercalations or lenses, and the lithology is mainly purple-red siltstone or sandy mudstone interspersed with gray-white tuffs or tuffaceous mudstone.

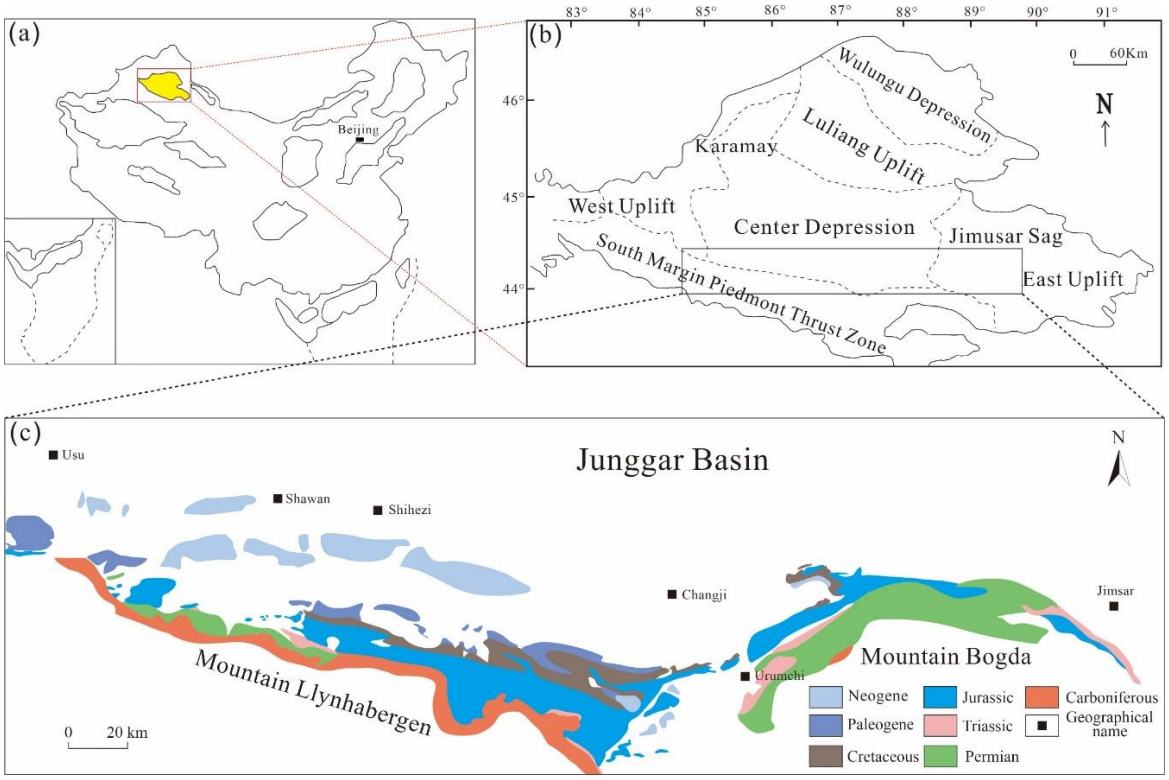

Figure 2. (a) Geographical position of Junggar Basin in China; (b) Tectonic position of the southern margin of E Junggar Basin; (c) Geological map of the southern margin of Junggar Basin.

3. Sampling and Methods

3.1. Samples

The experimental samples required for this study are selected from the cores and field outcrops of the Upper Triassic Yanchang Formation in the Ordos Basin (Figure 1) and the Middle Permian Jingjingzigou Formation in the southern margin of the Junggar Basin (Figure 2). Moreover, the samples are prepared according to different experimental requirements.

3.2. Methods

3.2.1. X-ray Diffraction Technology

X-ray diffraction (XRD) technology. It is a research tool that performs X-ray diffraction on a material, analyzing its diffraction pattern and obtaining information such as the composition of the material, the structure or morphology of the atoms or molecules inside the material. X-ray diffraction analysis is the main method to study the physical phase and crystal structure of substances. X-ray diffraction analysis, as a modern scientific method for the analysis of material structure and composition, has gradually been widely used in research and production in various disciplines. A D8

 doi:10.20944/preprints202312.0616.v1

DISCOVER system with Cu-Ka radiation at 40 Kv and 25 mA is selected for the XRD measurement tool. The samples are firstly ground into 200-250 mesh size powder, of which the ground powder is irradiated using the X-ray diffraction, and the relative contents of the different mineral components of the corresponding whole rock are derived from the positions and intensities of the diffraction peaks.

3.2.2. Field Emission Scanning Electron Microscope

The field emission scanning electron microscopy (FE-SEM) has ultra-high resolution. FE-SEM can do secondary electron image and reflection electron image observation and image processing of various solid sample surface morphology. FE-SEM can do secondary electron image and reflection electron image observation and image processing of various solid sample surface morphology. Combined with the high-performance X-ray spectrometer, it can simultaneously perform qualitative, semi-quantitative and quantitative analysis of the micro-area point-line elements of the sample surface and has the ability of comprehensive analysis of morphology and chemical components [49,50]. The most important feature of field emission scanning electron microscopy instrument is that it has ultra-high-resolution scanning image observation ability, especially the use of the latest digital image processing technology, providing high-power, high-resolution scanning images, is the most effective instrument for nanomaterials particle size testing and surface morphology observation of micron and nanoscale samples, and is more and more widely used in geological leaders [51,52].

3.2.3. Contact Angle Measurements

The contact angle is the angle between the tangent line made to the surface of the droplet and the solid-liquid surface when the liquid is stabilized by contact with the solid, after passing through the intersection of gas, liquid and solid phases. When dropping droplets on a solid plane at constant temperature and pressure, the droplets can automatically spread out on the solid surface or at an angle to the solid surface. There are many measurement methods to measure the contact angle, such as the suspension droplet method, tension measurement method, tilting plate method, Washburn method, and so on. The more commonly used method for measuring the contact angle of oil and gas reservoirs is the suspension droplet method. The suspension drop method is simple and easy to operate, with short testing time. However, the heterogeneity of the rock has a greater impact on it. Especially, unconventional reservoir mineral composition is complex and unevenly distributed, with heterogeneity of rocks. Based on the heterogeneous characteristics of the rock surface, the measurement angle varies widely, thus the method of averaging is generally utilized to represent the rock surface wettability. This study mainly used the German KRUSS DSA30S droplet analyzer to determine the contact angle between the solution and the sample surface. The instrument is equipped with a high-speed camera with a high-precision lens, which can record the dynamic spreading movement of different titration liquids on the shale surface through the high-speed camera, obtain a digital image of the shale surface, and realize semi-automatic retrieval of the droplet shape, determination and calculation of the contact angle through the system software.

3.2.4. Spontaneous Imbibition Measurements

Spontaneous imbibition is a common natural phenomenon occurring in porous media rocks. When porous media rocks and wetting liquids are in contact, the rocks will spontaneously draw in the wetting liquid under the action of capillary forces. Spontaneous imbibition is mainly dependent on the pore structure of porous media, capillary forces and rock-fluid interactions. Therefore, the pore connectivity and wettability of shale can be reflected by using spontaneous imbibition experiments. The more hydrophilic the rock is, the greater the capillary force and the faster the spontaneous imbibition rate, otherwise, the slower the rate. The spontaneous imbibition experimental apparatus includes electronic analytical balance, timer, hook, core holder, glass tray, adjustable elevator, computer, and so on. The experimental equipment is placed in a constant

Preprints (www.preprints.org) | NOT PEER-REVIEWED | Posted: 8 December 2023 doi:10.20944/preprints202312.0616.v1

temperature and humidity environment to reduce the influence of liquid evaporation as well as air flow on the core self-imbibition experiment.

3.3. Data Processing Methods

3.3.1. Plane Porosity Calculations

Using Image Pro Plus (IPP) software to statistically analyze the images captured by field emission scanning electron microscopy (FE-SEM) observation, the software can identify various pores and obtain the basic parameters of pore characteristics, such as area, perimeter, pore diameter, and so on. The software is able to identify the pores by using the grayscale value of each pixel in the image, combined with manual recognition and statistics to determine reasonable thresholds, thus accurately determining the basic parameters of the microscopic pores of the sample. The extraction of quantitative pore data by IPP image processing software can be divided into the following 3 steps (Figure 3): ① image reference scale setting; ② sample SEM image pore identification; ③ pore quantitative data extraction.

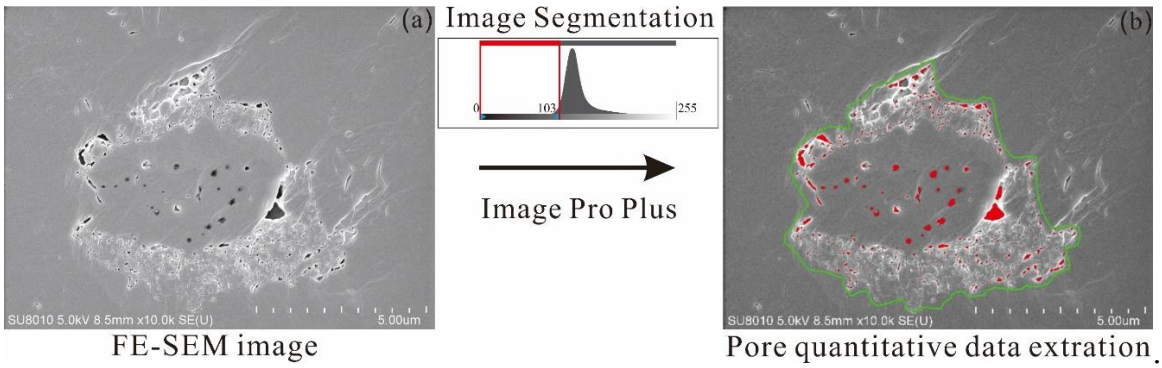

Figure 3. Pore extraction software process.

3.3.2. Wettability Parameter Calculation

The contact angle has been used as the most intuitive and effective method to evaluate interfacial wettability, by using the angles of deionized water and n-decane in contact with the sample surface to classify the degree of rock-fluid wettability. The contact angle has been used as the most intuitive and effective method to evaluate the interfacial wettability, and the degree of rock-fluid wettability has been classified using the angles of deionized water and n-decane when they are in contact with the sample surface: water wettability when the contact angle $\theta < 75°$; neutral wettability when $105° > \theta > 75°$; and oil wettability when $\theta > 105°$ [53], combining with previous work using contact angle to calculate wettability parameters to establish a set of wettability parameter discriminatory criteria [54]. The contact angle wettability parameter calculation equation is as follows:

$$CAI = \frac{90-\theta_w}{90} - \frac{90-\theta_O}{90} \quad (1)$$

where: CAI (Contact Angle Index) is the contact angle wettability parameter, θ_w is the water wettability angle, and θ_o is the oil wettability angle.

4. Results

4.1. Mineralogical Characteristics

The mineral composition of the tuffaceous shale samples from the Upper Triassic Yanchang Formation and the Middle Permian Jingjingzigou Formation is analyzed and determined. Based on the XRD analysis, it is shown that: according to XRD analysis, the tuffaceous mudstone of the Yanchang Formation is mainly composed of clay minerals (64.3 wt.% ~71.1 wt.%; average 74.5 wt.%),

Preprints (www.preprints.org) | NOT PEER-REVIEWED | Posted: 8 December 2023 doi:10.20944/preprints202312.0616.v1

followed by dolomite (0 wt.%~28.2 wt.%; average 14.1 wt.%), quartz (4.9 wt.%~8.9 wt.%; average 6.9 wt.%), plagioclase (2.5 wt.%~3.1 wt.%; average 2.8 wt.%), K-feldspar (0 wt.%~2.9 wt.%; 1.5 wt.% average), and siderite (0 wt.% ~0.4 wt.%; 0.2 wt.% average) with the least content.

The tuffaceous shales of the Jingjingzigou Formation consist mainly of ankerite (21.6 wt.%~71.5%; average 47.9 wt.%), plagioclase (17.5 wt.%~28.1 wt.%; average 21.9 wt.%) and clay minerals (0 wt.%~18 wt.%; average 9.2 wt.%), followed by quartz (3.9 wt.% ~9.7 wt.%; average 5.9 wt.%), calcite (0 wt.%~14.9 wt.%; average 5.0 wt.%), barite (6.9 wt.%~7.5 wt.%; average 4.8 wt.%), pyrite (0 wt.%~9.6 wt.%; average 3.2 wt.%), anhydrite (0 wt.%~4.8 wt.%; average 1.6 wt.%) and siderite (0 wt.%~1.5 wt.%; average 0.5 wt.%) with the least content.

The carbonate mineral contents of tuffaceous shale samples from the Middle Permian Jingjingzigou Formation (36.5 wt.%~71.5 wt.%, average52.8 wt.%) are comparatively higher than those of tuffaceous shale samples from the Upper Triassic Yanchang Formation (0 wt.%~28.2 wt.%, average 14.1 wt.%), furthermore, the carbonate minerals in the tuffaceous shales of the Jingjingzigou Formation are dominated by ankerite. Dolomites are mostly formed in high salinity (sufficient source of Mg^{2+}), high Mg/Ca ratio, as well as high pH (alkaline environment) in reducing water environments [55,56], therefore, the Middle Permian Jingjingzigou Formation tuffaceous shales have higher salinity in the sedimentary water column and alkaline water environment (Figure 4).

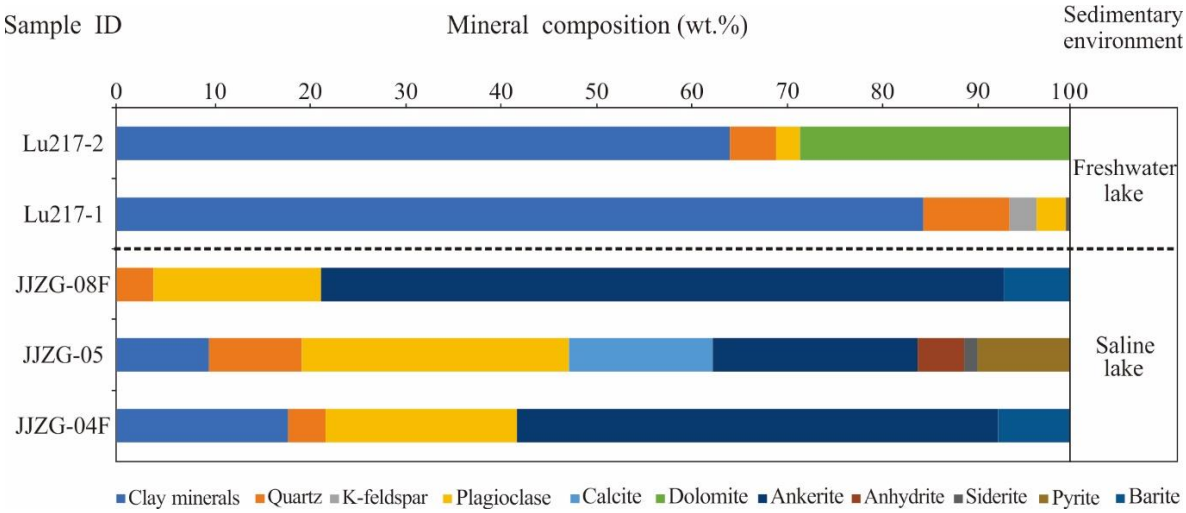

Figure 4. Whole-rock mineral composition in tuffaceous **shale**s of the Upper Triassic Yanchang Formation and Middle Permian Jingjingzigou Formation.

4.2. Pore Types

Tuffs or tuff-bearing reservoirs usually produce a large number of pores after the devitrification process [22]. Devitrification can be regarded as a kind of recrystallization, which is the process of rearranging the molecules and atoms inside the volcanic tuff that are originally loosely arranged, recrystallizing from vitreous silica to fine quartz, feldspar and other crystals, as well as a process of transforming from unstable components to stable components [16–18,23]. After the devitrified process, the tuffaceous particles get tightly arranged and produce devitrified pores, for example intergranular-intergranular pores, dissolution pores and microfractures.

The pore type and pore space characteristics can be determined using SEM, which enables the observation of the morphology and size characteristics of different pores within the tuffaceous reservoir. The SEM results show that the pore types and sizes in the tuff reservoirs within the Upper Triassic Yanchang Formation and the Middle Permian Jingjingzigo Formation in diverse, divided into (1) intergranular-intergranular pores, (2) dissolution pores, (3) microfractures, and (4) organic matter pores.

 doi:10.20944/preprints202312.0616.v1

4.2.1. Intergranular-Intercrystallite Pores

In the tuffaceous reservoir a large number of intergranular-intercrystallite pores, which are between clastic particles or authigenic particles, can be observed (Figure 5 a-b; g-h). These intergranular-intercrystallite pores are mainly the result of the transformation of components after vitreous devitrification to silicate crystalline or microcrystals, forming new minerals [57,58], as well as the reduction in volume relative to the original grains during the formation of new minerals, resulting in the development of a large number of microporosities between quartz and feldspar grains [59]. Intergranular-intercrystallite pores formed by devitrification are considered a very important pore type in tuffaceous reservoirs. These isolated intergranular-intercrystallite pores are gradually connected together under the modification of dissolution and other effects, thereby the pore connectivity in the reservoir to good, as well as to form an effective pore network. The shape of intergranular-intercrystallite pores varies, mainly forming polygonal and irregular shapes. The majority of intergranular-intercrystallite pores are of nanometer to micrometer diameter as well as the abundance of intergranular pores is the highest among all pore types.

By comparing the intergranular-intercrystallite pore development of the Upper Triassic Yanchang Formation tuffaceous shales (Figure 5 a-b) and the Middle Permian Jingjingzigou Formation tuffaceous shales (Figure 5 g-h). under scanning electron microscopy, it is concluded that the intergranular-intercrystallite pores of the Middle Permian Jingjingzigou Formation tuffaceous shales are more developed.

4.2.2. Dissolution Pores

In tuffaceous reservoirs, dissolution also has an effect on the physical properties of the reservoir. The feldspar content in the tuff reservoirs subjected to devitrification is relatively high. Since feldspar is easily dissolved, dissolution pores are mainly developed within the feldspar particles. Dissolution pores formed by devitrification are considered the most significant pore type in tuffaceous reservoirs. Due to the different degrees of dissolution, the shape of the mineral particles' dissolution pores is irregular and vary in size, showing round, sub-circular, curved or crescent shapes, with obvious corrosion marks on the edges of the dissolution pores (Figure 5 c; i-j). Due to the different degrees of dissolution, the shape of the mineral particles' dissolution pores is irregular and vary in size, showing round, sub-circular, curved or crescent shapes, with obvious corrosion marks on the edges of the dissolution pores.

By comparing the dissolution pores development of the Upper Triassic Yanchang Formation tuffaceous shales (Figure 5 c) and the Middle Permian Jingjingzigou Formation tuffaceous shales (Figure 5 i-j). under scanning electron microscopy, it is concluded that the dissolution pores of the Middle Permian Jingjingzigou Formation tuffaceous shales are more developed.

4.2.3. Microfractures

In tuffaceous reservoirs, well-developed microfractures or fractures are often observed (Figure 5 d-e; k). These microfractures usually develop along fractures or weak parts in mineral crystal fragments and exhibit irregular shapes or interlocking network structures. There are complex and diverse genetic types of microcracks, such as tectonics, ground stress, depositional environment, diagenesis, organic matter evolution, all influencing the development of microcracks [60−62] In tuffaceous reservoirs, microfractures within crystal fragments are usually caused by the release of large amounts of energy during magmatic eruptions, either due to a sudden drop in pressure and temperature when crystal fragments are sprayed from the subsurface, or microfractures from feldspar dissolution when geological fluids interact with minerals or tuffs to generate microfractures [14,21].

By comparing the microfractures development of the Upper Triassic Yanchang Formation tuffaceous shales (Figure 5 d,e) and the Middle Permian Jingjingzigou Formation tuffaceous shales (Figure 5 k). under scanning electron microscopy, it is concluded that the microfractures of the Middle Permian Jingjingzigou Formation tuffaceous shales are more developed.

Preprints (www.preprints.org) | NOT PEER-REVIEWED | Posted: 8 December 2023 doi:10.20944/preprints202312.0616.v1

4.2.4. Organic Matter Related Pores

Tuff reservoirs usually contain some amount of organic matter. Organic matter pores are generally developed in tuffaceous shales mainly and contraction joints at the edges of organic matter. The organic matter edge shrinkage seams are formed between the edges of organic matter and inorganic particles. The width of the shrinkage joints at the edges of organic matter in tuffs is usually less than 1 μm. The organic matter in tuffs is usually nonporous, except for a few joints at the contact of mineral grains (Fig5 i; l). Since organic matter pore space is a function of thermal maturity, the lack of pore space developed within organic matter in tuffs is mainly due to the low thermal maturity of samples in the study area (vitrinite reflectance <0.8%R_o). SEM images show that organic matter in tuffs is typically void-filled, suggesting that organic matter is interpreted as solid bitumen [63]. This solid bitumen may be residual oil that has migrated from potentially organic-rich shales to tuffs [63,64]. This type of organic matter usually blocks pre-existing intergranular pores and is therefore detrimental to reservoir quality [61]. The organic matter content in tuffs is limited and therefore the amount of pore space associated with organic matter is relatively low.

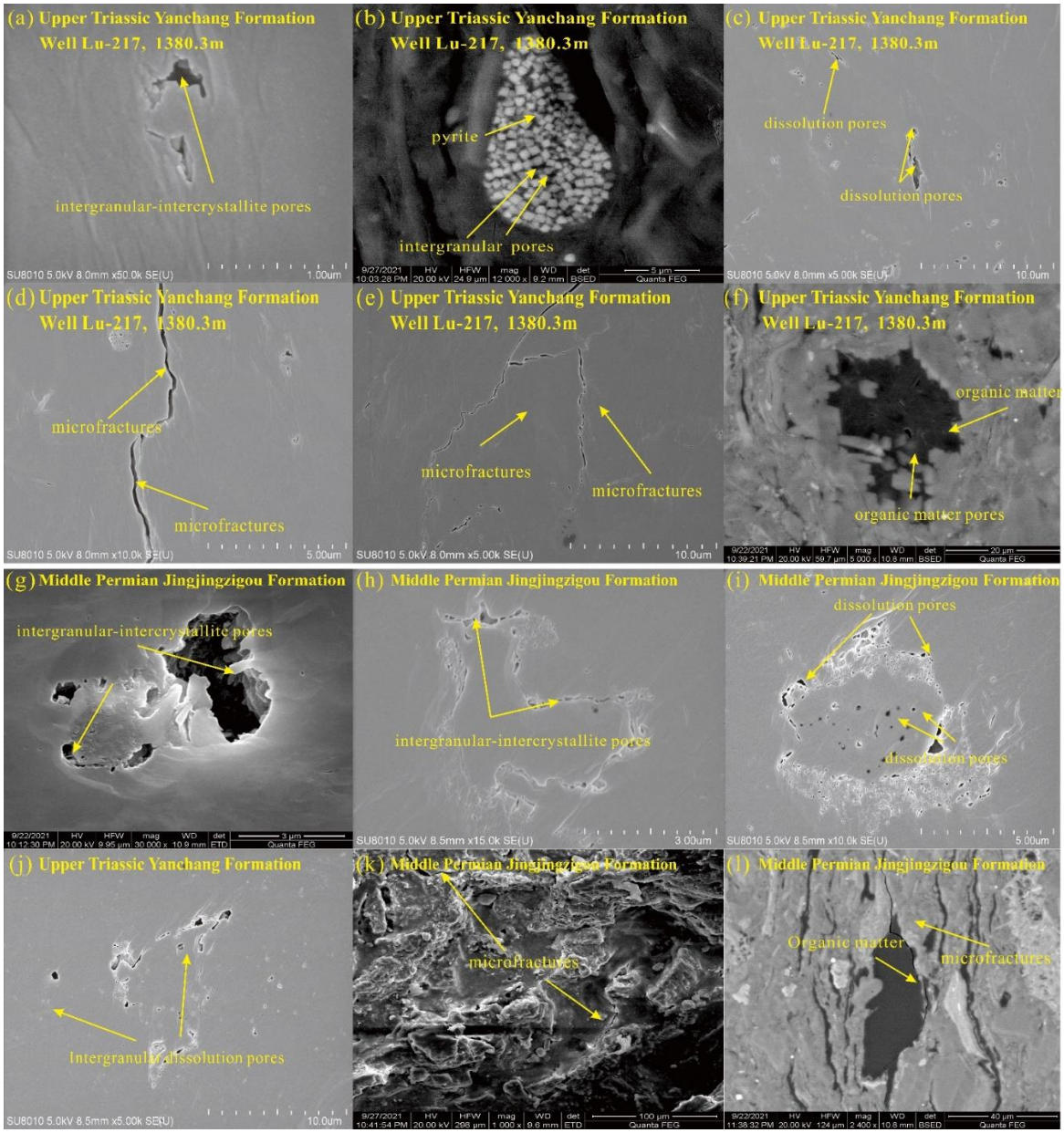

Figure 5. FE-SEM images of tuffaceous shale samples from the Upper Triassic Yanchang Formation (a-f) and Middle Permian Jingjingzigou Formation (g-l). (a) Typical intergranular-intercrystallite pore

 doi:10.20944/preprints202312.0616.v1

characteristics (few isolated devitrified pores, but signs of crystallite); (b) Development of pyrite and intergranular pores; (c) Typical dissolution pores; (d) Microfracture characteristics with a few dissolved pores; (e) Typical grain-edge microfracture characteristics (microscopic stylolites); (f) Organic matter pores; (g) Typical intergranular-intercrystallite pore with recrystallization; (h) Typical intergranular-intercrystallite pore pores and peripheral devitrified pores (with crystallite); (i) Dissolution pores (with crystallite phenomenon); (j) Dissolution pore; (k) Microfracture characteristics; (l) Organic matter filled in microfractures.

4.3. Spontaneous Imbibition Behavior

Spontaneous imbibition experiments of water and oil imbibition (n-decane) are performed on selected samples. In the experiment, there is a period of instability of about 1 min at the beginning, which is related to the open pore connectivity and wettability of the sample surface. After the instability period, a clear linear relation between the logarithm of the cumulative height of imbibition and the logarithm of the imbibition time of the samples is observed in the plot (Figure 6). The slope value of spontaneous imbibition can reflect the quality of pore connectivity of the samples.

The experimental results show that (Table 4.1): the spontaneous imbibition slope of deionized water for the Upper Triassic Yanchang Formation samples ranged from 0.310~0.330 (Figure 6 a-b), with an average of 0.320, and the spontaneous imbibition slope of n-decane ranged from 0.392~0.440 (Figure 6 a′-b′), with an average of 0.420. The spontaneous imbibition slope of deionized water for the Middle Permian Jingjingzigou Formation samples ranged from 0.359~0.366 (Figure 6 c-d), with an average of 0.349, and the spontaneous imbibition slope of n-decane is 0.460~0.500 (Figure 6 c′-d′), with an average of 0.480.

Table 4.1. Experimental results of spontaneous imbibition of tuffaceous shale samples from the Upper Triassic Yanchang Formation and Middle Permian Jingjingzigou Formation.

Sample ID	Spontaneous imbibition (deionized water) slope	Spontaneous imbibition (n-decane) slope
Lu217-1	0.330	0.392
Lu217-2	0.310	0.440
JJZG-05F	0.366	0.460
JJZG-08F	0.359	0.500

Preprints (www.preprints.org) | NOT PEER-REVIEWED | Posted: 8 December 2023 doi:10.20944/preprints202312.0616.v1

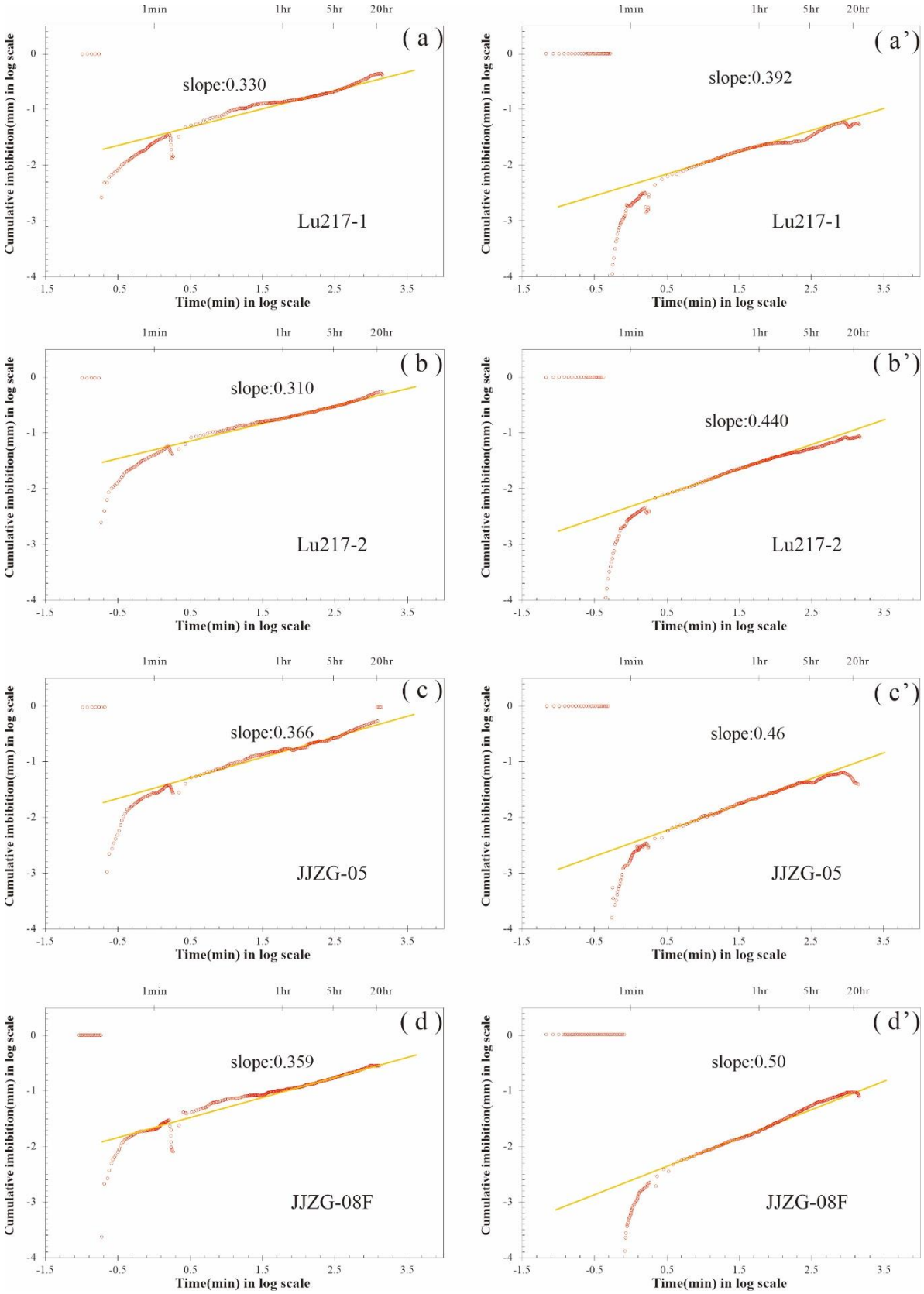

Figure 6. Spontaneous imbibition results of tuffaceous shale samples from the Upper Triassic Yanchang Formation and Middle Permian Jingjingzigou Formation. (a-d) Images of spontaneous imbibition results of deionized water from tuffaceous shale samples of the Upper Triassic Yanchang and Middle Permian Jingjingzigou Formations; (A-D) images of spontaneous imbibition results of n-

Preprints (www.preprints.org) | NOT PEER-REVIEWED | Posted: 8 December 2023 doi:10.20944/preprints202312.0616.v1

decane from tuffaceous shale samples of the Upper Triassic Yanchang and Middle Permian Jingjingzigou Formations.

As shown by the above spontaneous imbibition results, the slope of spontaneous imbibition of deionized water (0.366~0.359) and the slope of spontaneous imbibition of n-decane (0.460~0.500) of the Middle Permian Jingjingzigou Formation samples are respectively greater than the slope of spontaneous imbibition of deionized water (0.310~0.330) and the slope of spontaneous imbibition of n-decane (0.392~0.440) of the Upper Triassic Yanchang Formation samples. The slope of oil imbibition is greater than the slope of water imbibition in both samples of the Jingjingzigou Formation and the Yanchang Formation, suggesting that both samples are more facilitative for oil flow and enrichment, with the more obvious effect in the Jingjingzigou Formation. Overall, the slope value of spontaneous imbibition of the samples from the Jingjingzigou Formation is larger than that of the samples from the Yanchang Formation, which shows better internal pore connectivity.

4.4. Wettability Characteristics

The contact angles of deionized water and n-decane of Upper Triassic Yanchang Formation samples and Middle Permian Jingjingzigou Formation samples are obtained by the contact angle measurement experiments.

The experimental results show that the deionized water contact angles of the Upper Triassic Yanchang Formation tuffaceous shale samples range from 71.82°~75.07°, with an average of 73.26°, whereas the n-decane contact angles range from 16.07°~18.14°, with an average of 16.92°. The deionized water contact angle of the Middle Permian Jingjingzigou Formation tuffaceous shale samples ranges from 67.38°~78.80°, with an average of 73.05°, whereas the n-decane contact angle of the samples ranges from 5.49°~17.28°, with an average of 12.57°. According to the wettability criteria, combined water and oil wettability of the Upper Triassic Yanchang Formation and Middle Permian Jingjingzigou Formation tuffaceous shale samples, the Jingjingzigou Formation samples are more oil wettable than the Yanchang Formation samples.

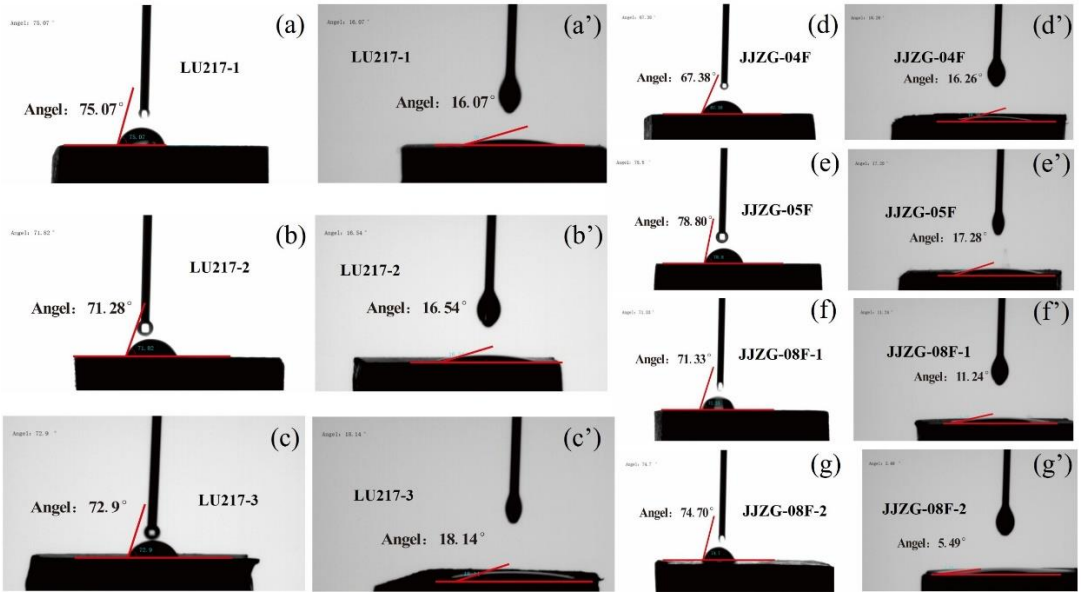

Figure 7. Determination of wettability angle of tuffaceous shale samples from the Upper Triassic Yanchang Formation and Middle Permian Jingjingzigou Formation. (a-c) Images of deionized water contact angle results of tuffaceous shale samples from the Upper Triassic Yanchang Formation; (d-g) images of deionized water contact angle results of tuffaceous shale samples from the Middle Permian Jingjingzigou Formation; (a'-c') images of n-decane contact angle results of tuffaceous shale samples from the Upper Triassic Yanchang Formation; (d'-g') images of n-decane contact angle results of tuffaceous shale samples from the Middle Permian Jingjingzigou Formation.

 doi:10.20944/preprints202312.0616.v1

Based on the measured results of deionized water contact angle and n-decane contact angle of the samples, combined with the wettability parameter calculation equation (1), the wettability parameters are calculated for the Upper Triassic Yanchang Formation samples and the Middle Permian Jingjingzigou Formation tuffaceous shale samples (Table 4.2)

Table 4.2. Wettability parameters calculation method and judgment criteria.

Measurement methods	Measurement parameters and calculation methods	Judgment Criteria		
		Water wetting	Neutrally wetting	Oil wetting
Contact angle method	θ	θ≤75°	75°<θ<105°	θ>105°
CAI	CAI=(θ_o-θ_w)/90	CAI≥-0.67	-1<CAI<-0.67	CAI≤-1

The calculation results show (Table 4.3): the wettability parameters of tuffaceous shale samples from the Yanchang Formation range from -0.66~-0.61, with an average of -0.63; the wettability parameters of tuffaceous shale samples from the Jingjingzigou Formation range from -0.77~-0.57, with an average of -0.67. According to the standard for judging the wettability parameters and combining the performance of water and oil wettability angles of tuffaceous shale samples from the two areas, the samples from the Yanchang Formation are more water wettable than those from the Jingjingzigou Formation. The samples of the Jingjingzigou Formation are more oil-wetted than those of the Yanchang Formation (Figure 8).

Table 4.3. Wetting angle and wettability parameters of tuffaceous shale samples from the Upper Triassic Yanchang Formation and Middle Permian Jingjingzigou Formation.

Sample ID	Water wetting angle（θ_w/°）	Average value of water wetting angle	Oil wetting angle（θ_w/°）	Average value of oil wetting angle	wettability parameters (CAI)	Wettability	Average value of wettability parameters
Lu-217-1	75.07	73.26	16.07	16.92	-0.66	hydrophilic	-0.63
Lu-217-2	71.82		16.54		-0.61	hydrophilic	
Lu-217-3	72.9		18.14		-0.60	hydrophilic	
JJZG-04F	67.38		16.26		-0.57	hydrophilic	
JJZG-05F	78.8	73.1	17.28	12.57	-0.68	oleophilic	-0.67
JJZG-08F-1	71.33		11.24		-0.67	oleophilic	
JJZG-08F-2	74.7		5.49		-0.77	oleophilic	

Preprints (www.preprints.org) | NOT PEER-REVIEWED | Posted: 8 December 2023 doi:10.20944/preprints202312.0616.v1

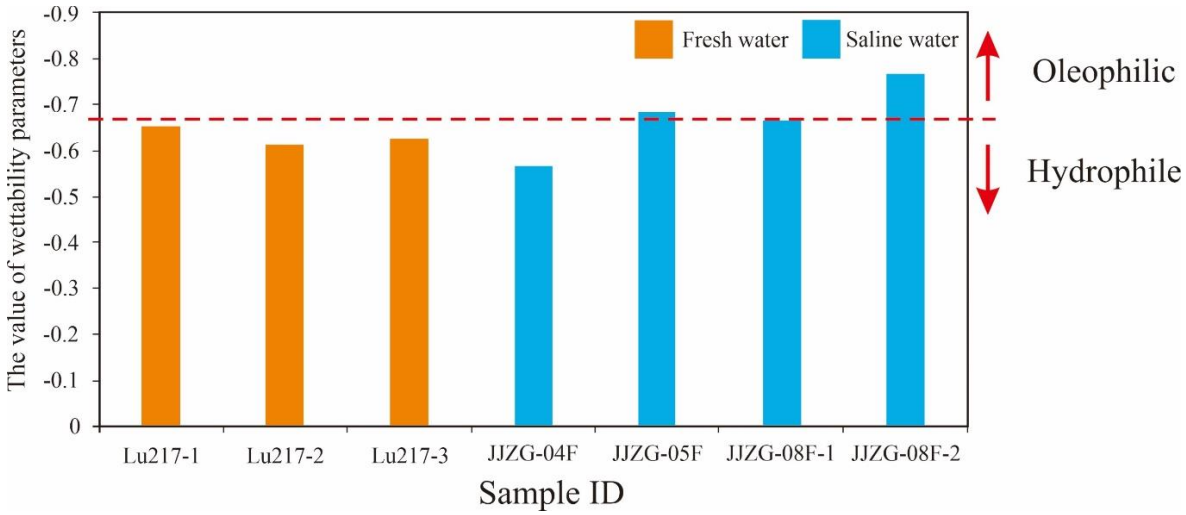

Figure 8. Histograms of wetting angle parameters of Upper Triassic Yanchang Formation samples and Middle Permian Jingjingzigou Formation tuffaceous shale samples.

5. Discussion

5.1. Mechanism for Differentiation of Freshwater and Saline Water Devitrification Degree

Volcanic clastic material is a sediment with a mixture of plastic, rigid and semi-plastic particles, mainly composed of microscopic vitric fragments, crystal fragments (feldspar, quartz, and so on) and rock fragments in an aggregate dominated by aluminosilicate minerals, containing small amounts of clay minerals and pyrite [66,67]. Since the vitreous thermodynamic properties of volcanic clastic materials are very instable, vitreous components such as vitric fragments can be easily converted into crystals, namely devitrification [68]. During the burial process, with the change of environmental conditions such as temperature, pressure and fluid properties, the devitrification and dissolution carried out within the volcanic clastic materials are affected to different devitrification degrees, which are mainly reflected in the crystallization, dissolution and reprecipitation of volcanic materials and the migration and transformation of ions. In the above process, some components of the volcanic clastic materials migrate out of the local system with the formation water, while the remaining components crystallize or precipitate to form new crystallite or microcrystalline authigenic minerals, meanwhile the overall volume of the tuff decreases and a large number of pores are formed, meaning devitrification pores. Devitrification pores are usually micro-nanometer pores, as well as a large number of pores and good connectivity within a highly devitrified reservoir, which can be used as an important storage space in tuffaceous reservoirs [69]. Microcrystalline quartz formed by devitrification can be observed under SEM, with a large number of intercrystallite pores formed between these microcrystalline quartz particles, capable of serving as an effective storage space for oil and gas. Devitrification is influenced by many factors, such as temperature, pressure, organic acids, and formation water action. During diagenesis, with the increase of temperature and pressure, the activity and rearrangement rate of thermodynamically unstable vitreous internal masses in tuff reservoirs are accelerated, which is favorable for the positive proceeding of devitrification and conversion to crystals, such as microcrystalline quartz, feldspar and zeolite [59].

The degree of devitrification is significantly affected by the action of organic acids, during devitrification many silicate minerals are produced, which will be dissolved by complexation with organic acids under acidic conditions and carried away by pore fluids, shifting the chemical equilibrium of the whole devitrification to the positive reaction direction and promoting devitrification. The dynamic process of volcanic material and formation water has an important influence on the devitrification process of volcanic material. Alkaline formation water can cause the dissolution of quartz and accelerate the reduction of Si in the reservoir, which makes volcanic vitreous dissolve and devitrification [71] and form a large number of authigenic minerals with other

 doi:10.20944/preprints202312.0616.v1

metal ions, such as K-feldspar, zeolite, montmorillonite, illite, chlorite, and so on [70]. With the continuous precipitation of alkali metal ions such as Na, K, Ca, Mg, Fe, the volcanic materials contain only Si and O, and finally crystallize to form authigenic quartz, which can promote the devitrification process.

According to XRD analysis, carbonate minerals occupy a high proportion (36.5 wt.%~71.5wt.%, average 52.8wt.%) in tuffaceous shale samples of the Middle Permian Jingjingzigou Formation, moreover, the carbonate mineral composition is mainly ankerite. Following the International Mineralogical Association guidelines [72] when Fe replaces more than half of the Mg in the dolomite lattice, it is called ankerite. As a kind of dolomite, the formation environment of iron dolomite is similar to that of dolomite, which is a saline environment with high water salinity and high pH.

Based on previous studies, it is shown that the paleoclimate was warm and humid during the deposition of the Upper Triassic Yanchang Formation in the Ordos Basin, with the water bodies forming a freshwater environment [73], furthermore, the tuff rich Chang 7 member was formed at the peak of lake basin development and the most extensive lake area in the whole basin [38]. However, the depositional period of the Jingjingzigou Formation on the southern margin of the Junggar Basin changed from a wet paleoclimate to a seasonal dry and hot climate, and some terrestrial deposits in the fluvial-delta-lacustrine facies were affected by the climate shift resulting in an overall shallowing of the water column and an increase in water salinity to form a saline lake basin background dominated by sedimentary environment [48]. Therefore, in a significantly different depositional context, the samples of the Upper Triassic Yanchang Formation and the samples of the Middle Permian Jingjingzigou Formation are subject to significant differences in devitrification, in addition, the pore structure characteristics and wettability of the samples from the two regions are significantly different under the influence of the degree of devitrification.

The devitrification effect is obvious for the transformation of the pore-forming matrix. The IPP technique is used to extract the three types of intergranular-intercrystallite, dissolved pores and microfractures in the SEM photographs of each sample and calculate the corresponding plane porosity (Figure 9). Using the plane porosity to reflect the degree of pore development within the reservoir under the influence of devitrification. The results show (Figure 10) that the maximum plane porosity of intergranular-intercrystallite pore of the Upper Triassic Yanchang Formation samples can reach 0.81%, the maximum plane porosity of dissolved pore can reach 0.43% and the maximum plane porosity of microfracture can reach 1.14%, respectively, and the pore development of devitrified degree of samples is not well developed and the devitrified effect is weak. Under the same field of vision, the sample of the Middle Permian Jingjingzigou Formation has a maximum of 2.91% of intergranular-intercrystallite pore plane porosity, 2.21% of dissolved pore plane porosity and 2.60% of microfracture plane porosity. The samples have well-developed devitrified pores and are obviously subject to devitrified effect. The comparison of the porosity of three types of these samples, including intergranular-intercrystallite pores, dissolved pores and microfractures, in the two regions shows that the pore development of the Middle Permian Jingjingzigou Formation samples is better, with a higher degree of devitrification. After devitrification, plastic vitric pyroclastic in tuff is converted into microcrystalline quartz and feldspar. Quartz and feldspar particles have good compaction resistance and can prevent pores from being destroyed by compaction so as to provide good support in shale reservoirs. The content of quartz-feldspathic in samples from the Middle Permian Jingjingzigou Formation (21.5 wt.%~37.8 wt.%; average 27.8 wt.%) is greater than that of quartz-feldspathic in samples from the Upper Triassic Yanchang Formation (7.4 wt.%~14.8 wt.%; average 11.2 wt.%), indicating that the mineral skeleton of the samples of the Middle Permian Jingjingzigou Formation is more well supported and provides good protection for the pore space. The above two factors together are important reasons for the degree of devitrification to control the pore development and pore preservation ability of tuffaceous reservoirs.

Preprints (www.preprints.org) | NOT PEER-REVIEWED | Posted: 8 December 2023 doi:10.20944/preprints202312.0616.v1

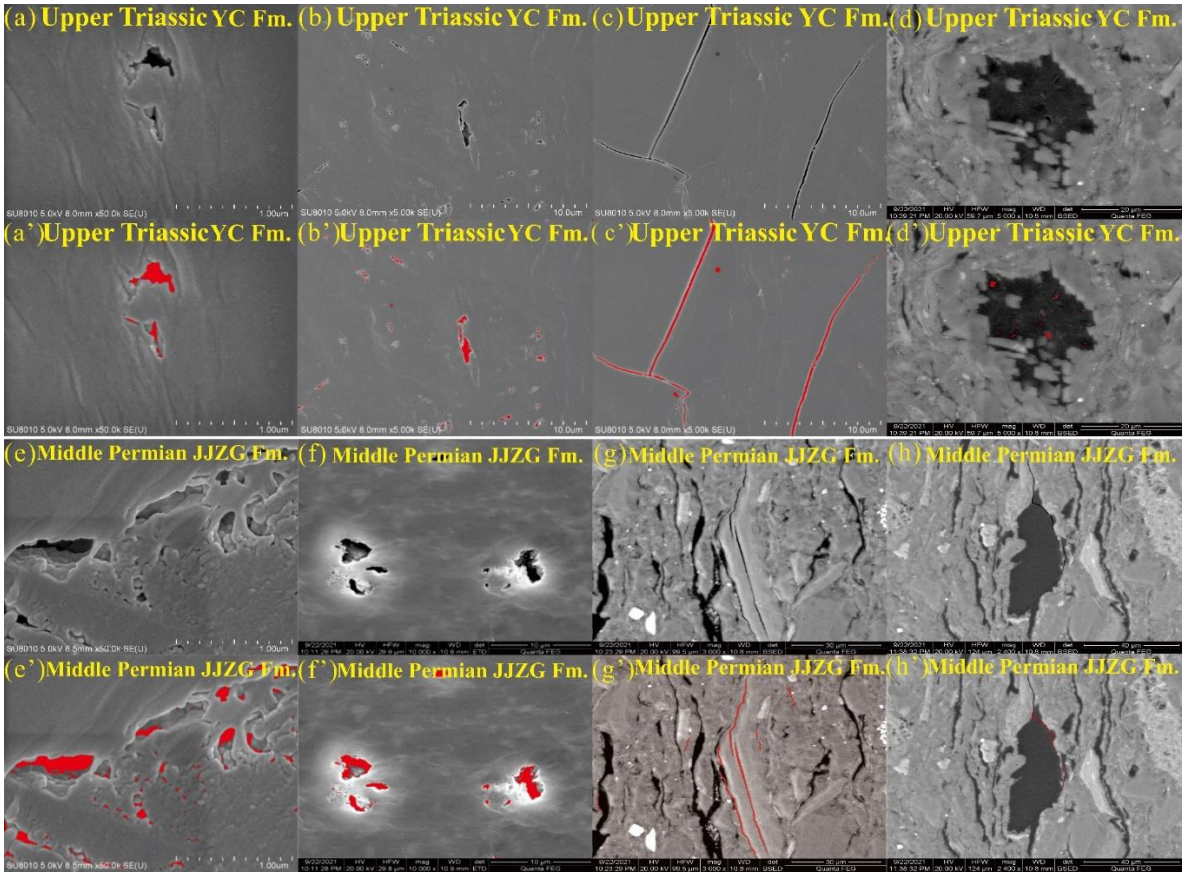

Figure 9. Porosity extraction of tuffaceous shales pore surfaces of the Upper Triassic Yanchang Formation and Middle Permian Jingjingzigou Formation.

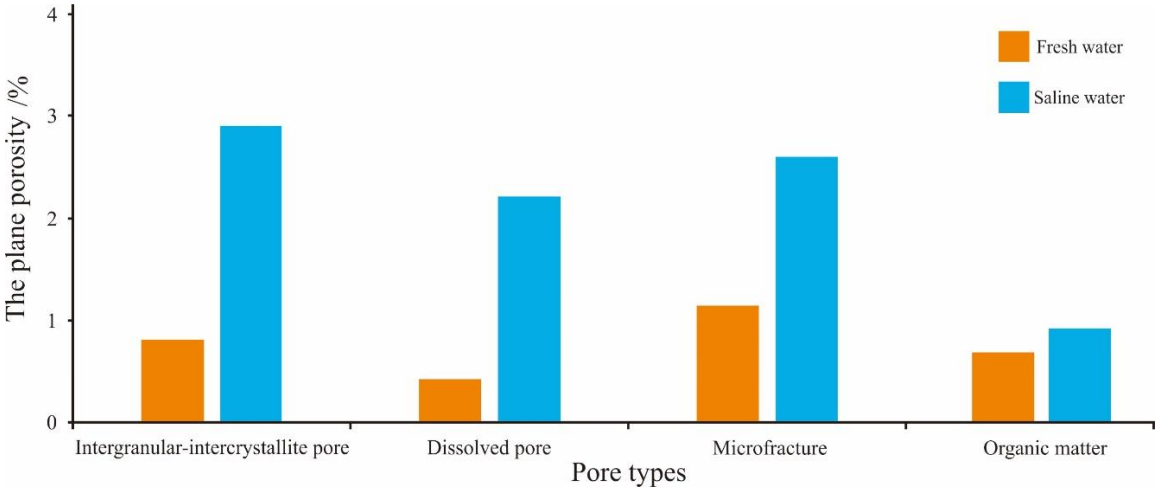

Figure 10. Histogram of plane porosity of tuffaceous shale samples in different depositional environments.

5.2. Control of Pore Structure Characteristics and Interfacial Wetting Effects by Differential Devitrification

The samples of the Middle Permian Jingjingzigou Formation are subject to a higher degree of devitrified action than those of the Upper Triassic Yanchang Formation. The spontaneous imbibition experiments show that the spontaneous imbibition slope of deionized water (0.366~0.359) and the spontaneous imbibition slope of n-decane (0.460~0.500) of the Middle Permian Jingjingzigou Formation samples are greater than the spontaneous imbibition slope of deionized water (0.310~0.330) and the spontaneous imbibition slope of n-decane (0.392~0.440) of the Upper Triassic

 doi:10.20944/preprints202312.0616.v1

Yancheng Formation samples. This shows that the pore connectivity of the Middle Permian Jingjingzigou Formation tuffaceous shales is better than that of the Upper Triassic Yanchang Formation tuffaceous shales. The higher spontaneous imbibition slope of the sample from the Middle Permian Jingjingzigou Formation indicates that the tuff-bearing reservoir has a higher degree of devitrification and better pore connectivity. After devitrification, a large number of intergranular pores and dissolution-associated pores are formed in the Middle Permian Jingjingzigou Formation tuffaceous shales, forming an effective pore network under the communication effect of microfractures, which serves as a imbibition channel for formation fluids and organic fluids and also provides fluid exchange space for tuff dissolution, accelerating the process of devitrification and dissolution around the microfractures and positively promoting the formation of effective pores and the connectivity between various pores. In contrast, the devitrification of tuffaceous shales of the Upper Triassic Yanchang Formation is weak, the development of devitrification pores in the reservoir is limited, making it difficult to form an effective pore network, so that the effective imbibition channels of geological and organic fluids are difficult to form, which reduces the process of devitrification and dissolution of tuff and makes the pore connectivity in the reservoir lower. Therefore, the pore connectivity of the Middle Permian Jingjingzigou Formation tuffaceous shales is better than that of the Upper Triassic Yanchang Formation tuffaceous shales.

According to the spontaneous imbibition experiment, it is concluded that the spontaneous imbibition slope of n-decane is greater than the spontaneous imbibition slope of deionized water for the tuffaceous shales of the Middle Permian Jingjingzigou Formation and the tuffaceous shales of the Upper Triassic Yanchang Formation (Figure 11), besides, the difference between the spontaneous imbibition slope of deionized water (0.366~0.359) and the spontaneous imbibition slope of n-decane (0.460~0.500) is greater in the tuffs of the Middle Permian Jingjingzigou Formation. It indicates that the interfacial wettability within the tuff reservoir has been changed after devitrification, moreover, the difference in the degree of devitrification affects the degree of change of interfacial wettability within the reservoir. The degree of devitrification of tuffaceous shales in the Middle Permian Jingjingzigou Formation is obvious. When the tuff components in the reservoir are devitrified, the hydrophilic substances such as vitreous matter are reduced, which changes the wetting at the liquid-solid interface, meanwhile, the various types of pores formed by devitrified effect led to similar capillary force in the reservoir, which is favorable for oil retention, so that the wettability of the tuffaceous shale interface is changed from hydrophilic to oleophilic, which provides effective transport channels for hydrocarbon fluids. In contrast, the Upper Triassic Yanchang Formation tuffaceous shales are subject to a low degree of devitrification, which still retains a large amount of hydrophilic components such as vitreous matter in the tuff, with less formation of devitrification pores and difficulty for hydrocarbon fluids to enter into, making the degree of interfacial wettability changed limited. The water contact angle (Figure 7 d-g) of the Middle Permian Jingjingzigou Formation tuffaceous shale samples is approximately equal to that of the Upper Triassic Yanchang Formation tuffaceous shale samples (Figure 7 a-c), and the oil contact angle (Figure 7 d’-g’) of the Middle Permian Jingjingzigou Formation tuffaceous shale samples is smaller than that of the Upper Triassic Yanchang Formation tuffaceous shale samples (Figure 7 a’-c’), indicating that the Middle Permian Jingjingzigou Formation tuffaceous shales are more oleophilic. According to the wettability parameters of each sample and the wettability classification criteria, the Middle Permian Jingjingzigou Formation samples are more oil-wettable and the Upper Triassic Yanchang Formation samples are water-wettable. Based on the statistical results of the spontaneous imbibition and wettability parameters of the Middle Permian Jingjingzigou Formation tuffaceous shales and the Upper Triassic Yanchang Formation tuffaceous shales (Table 4.3), combined with the plane porosity of the three types of pores affected by devitrification (devitrified pores, dissolution pores and microfractures) of the Middle Permian Jingjingzigou Formation tuffaceous shales and the Upper Triassic Yanchang Formation tuffaceous shales, it is obvious that the higher the value of the plane porosity, the higher the value of the spontaneous imbibition slope and the smaller the value of the wettability parameter Moreover, all three types of pores affected by devitrification reflect the same pattern and regularity (Figure 12). In other words, the higher the degree of devitrification and the

Preprints (www.preprints.org) | NOT PEER-REVIEWED | Posted: 8 December 2023 doi:10.20944/preprints202312.0616.v1

more developed the devitrification pores are, the better the pore connectivity of the tuffaceous shales, the more oleophilic the sample is, which is more favorable to the tuff-bearing reservoir space for oil and gas storage. Therefore, the difference of devitrification has a significant influence on the pore structure characteristics and interfacial wettability. The interfacial wettability of tuffaceous shales media of the Middle Permian Jingjingzigou Formation is more inclined to oil wetting than that of tuffaceous shales media of the Upper Triassic Yanchang Formation due to the difference in the degree of devitrification.

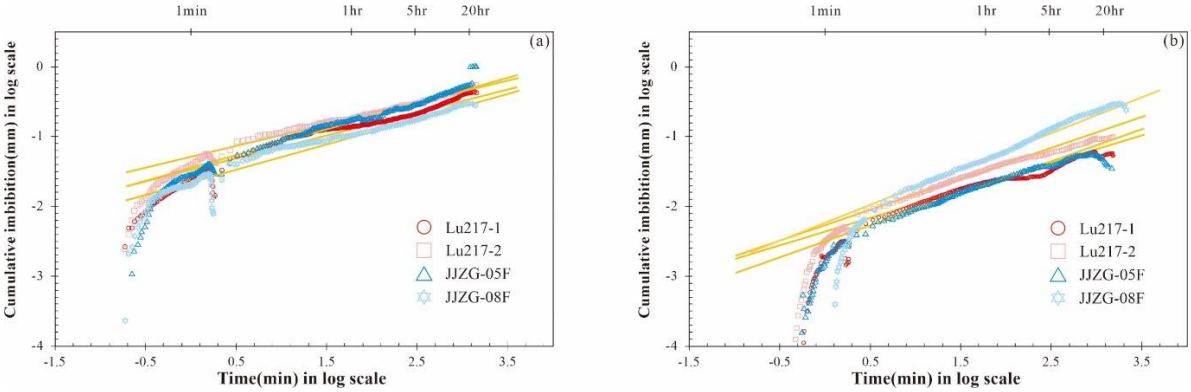

Figure 11. (a) Spontaneous imbibition results of deionized water from tuffaceous shale samples of the Upper Triassic Yanchang and Middle Permian Jingjingzigou Formations; (b) spontaneous imbibition results of n-decane from tuffaceous shale samples of the Upper Triassic Yanchang and Middle Permian Jingjingzigou Formations.

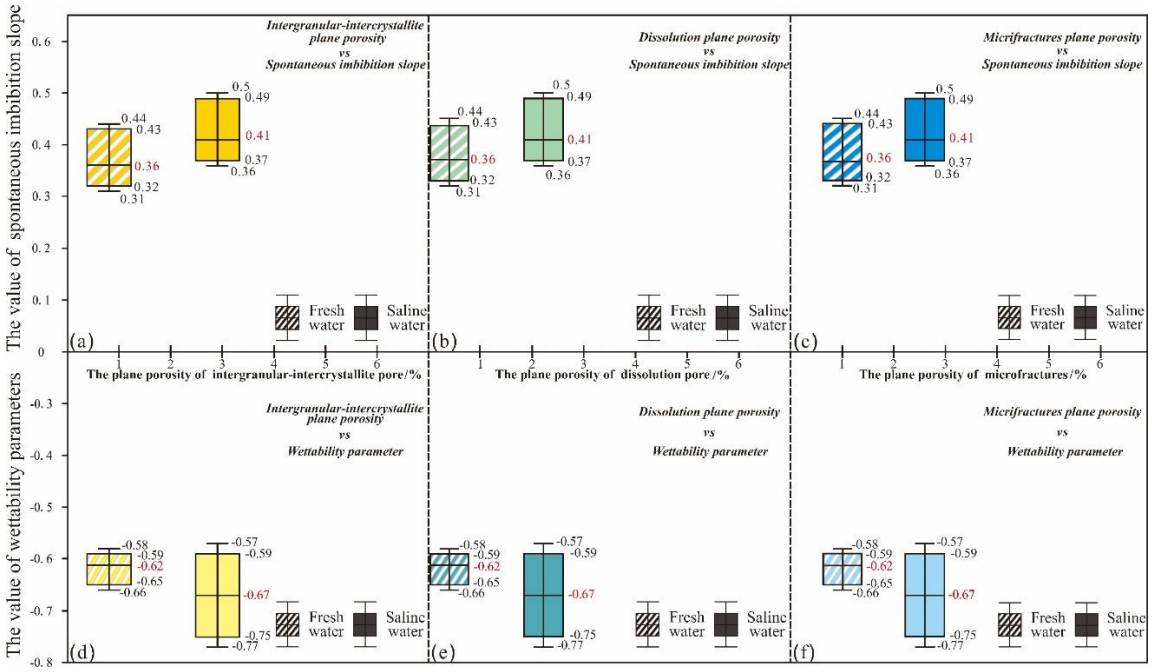

Figure 12. Box plots of devitrified pores, dissolution pores, microfractures with spontaneous imbibition and wettability parameters under different deposition environments.

5.3. Comprehensive Model of Reservoir Differentiation between Fresh-Water and Saline Lacustrine Tuffaceous Shale Formation

Based on the analysis of the mineral composition, pore type, pore connectivity characteristics and interfacial wettability of the Upper Triassic Yanchang Formation and Middle Permian Jingjingzigou Formation samples, it provides clues to the degree of devitrification in two different

Preprints (www.preprints.org) | NOT PEER-REVIEWED | Posted: 8 December 2023 doi:10.20944/preprints202312.0616.v1

environments, freshwater and saline lake basins, inferring that devitrification differences affect the pore structure and interfacial wettability within the reservoir. To better understand the effect of the difference in the degree of devitrification on reservoir pore connectivity and interfacial wettability as well as reservoir formation differences, a conceptual model of the two sets has been constructed (Figure 13).

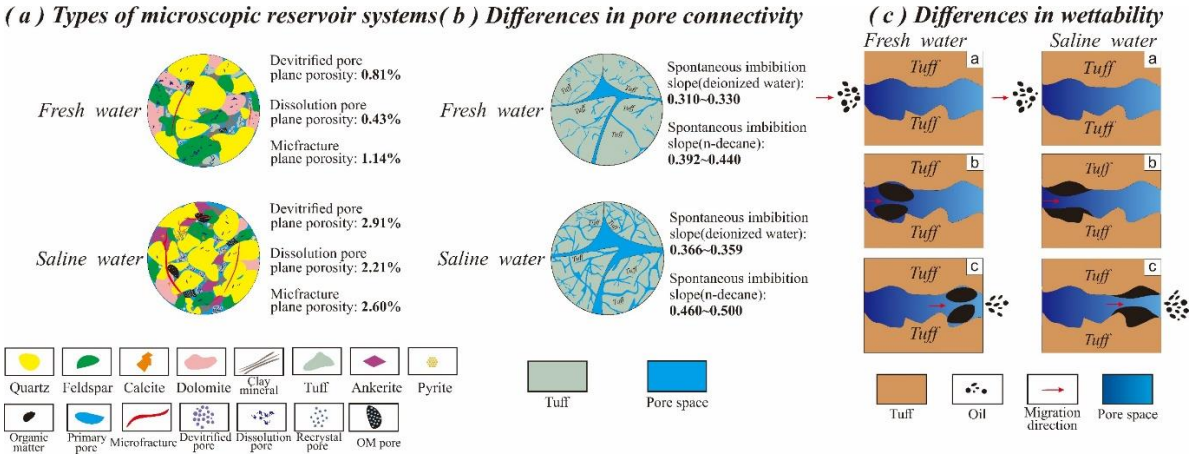

Figure 13. Comprehensive and conceptual models illustrating difference of devitrification in the Upper Triassic Yanchang Formation and the Middle Permian Jingjingzigou Formation.

The tuffaceous shales of the Upper Triassic Yanchang Formation differ significantly from the tuffaceous shales of the Middle Permian Jingjingzigou Formation in terms of reservoir formation mode. The low degree of devitrification in the tuffaceous shale samples of the Upper Triassic Yanchang Formation makes the devitrification pores formed in the tuff few and dispersed, mostly isolated pores. The dissolution is weak, forming fewer dissolution pores. Few microfractures, many isolated pores lack the communication of microfractures, which make it difficult for microfractures to form an effective pore network with primary pores, devitrified pores and dissolved pores, thus poor pore connectivity within the reservoir. The weak devitrified degree leads to the high content of vitreous matter in the reservoir, low pore development, restricted interfacial wettability change, as well as poor mobility of hydrocarbon fluids in the pore space of devitrified genesis. Therefore, the low degree of devitrification has little effect on the pore structure characteristics of tuffaceous shales and the wettability modification of the interface.

The Middle Permian Jingjingzigou Formation tuffaceous shales have a high degree of devitrified action, with a large number of devitrified pores formed in the tuff component. Tuffaceous shales are subject to obvious dissolution, which can further develop devitrification pores. Microfractures are well developed in tuff reservoirs subject to obvious devitrification, which can be used as effective fluid percolation channels, forming an effective pore network with primary pores, devitrification pores and dissolution pores in the reservoir. The pore connectivity gradually becomes better. The high degree of devitrification leads to high content of feldspathic quartzite in the reservoir, the development of pore space, the large reduction of hydrophilic minerals such as vitrinite, and the significant improvement of interfacial wetting effect. Hydrocarbon fluids can flow in the pore space formed by tuff devitrification. The wetting of the fluid-rock interface in the reservoir with a high degree of devitrification has an obvious reversal, which is gradually oleophilic and facilitates the retention of hydrocarbon substances such as shale oil, which also helps the reversal of the wetting of the mixed tuffaceous shales medium interface. Therefore, the high degree of devitrification has a significant effect on the pore structure characteristics of tuffaceous shales and the wettability of the interface.

 doi:10.20944/preprints202312.0616.v1

6. Conclusions

The degree of devitrification of the Upper Triassic Yanchang Formation in Ordos Basin is quite low, the development of devitrification pores in the reservoir is few, the dissolution is not obvious, there are few dissolution pores, few microfractures, isolated pores lack the communication of microfractures, thus the connectivity of pores in the reservoir is poor. The degree of devitrified leads to high content of vitreous matter in the reservoir, low pore development, restricted change of interfacial wettability, limited mobility of hydrocarbon fluids in the pore space of devitrified genesis. The tuffaceous shales of the Middle Permian Jingjingzigou Formation in the Junggar Basin have a high degree of devitrification, a large number of devitrification pores, obvious dissolution, and well-developed dissolution pores; the microfractures are well developed. The pores formed by devitrification in the reservoir can form an effective pore network with the native pores, resulting in well-connected pores. The high degree of devitrification makes the interfacial wettability effect in the reservoir improved significantly, hydrocarbon fluids can flow in the pore space formed by tuff devitrification, wettability of fluid-rock interface in the reservoir is reversed significantly, gradually oleophilic, which is favorable to the retention of shale oil and other hydrocarbon substances, as well as contributes to the reversal of wettability of the interface of mixed tuffaceous shales media.

The differential reservoir formation of the Upper Triassic Yanchang Formation in the Ordos Basin and the Middle Permian Jingjingzigou Formation in the southern margin of the Junggar Basin is mainly controlled by devitrification. The Upper Triassic Yanchang Formation tuffaceous shales have a warm and humid deposition period, with fresh water as the water body environment which limits the devitrification, resulting in high content of clay minerals and vitreous with lower content of quartz and feldspar, which limits the development of devitrification pores; the primary pores in the reservoir are filled by volcanic debris materials (such as vitreous), making the pore connectivity in the reservoir poor; the presence of vitreous and other hydrophilic materials leads to the wettability of the reservoir hydrophilic, which is not conducive to the formation of shale oil reservoirs. The Middle Permian Jingjingzigou Formation tuffaceous shales are subject to significant devitrification, with higher quartz and feldspar contents, more devitrification pores in the reservoir, more carbonate minerals, which promote the development of dissolution pores and obvious microfracture development, thus the three types of pores together build a good pore-fracture network in the reservoir, which greatly improves the space for reservoir storage of oil and gas. After devitrification, the hydrophilic substances such as vitreous in the reservoir are reduced and the wettability is changed, gradually moving from hydrophilic to oleophilic, providing effective transport channels for hydrocarbon fluids and facilitating the preservation of oil and gas in tuff-bearing reservoirs.

In this study, it compared the reservoir space characteristics and reservoir wettability characteristics of the Upper Triassic Yanchang Formation in the Ordos Basin and the Middle Permian Jingjingzigou Formation in the southern margin of the Junggar Basin, revealed the differential reservoir formation mechanism of the two sets of tuffaceous shales, which laid the foundation for determining the main control factors of shale oil enrichment. Finally, the differential reservoir formation model of terrestrial shales is established, which provides a theoretical basis for the commercial development of domestic terrestrial shale oil.

Acknowledgments: This work was mainly financed by the Open Project Fund of State Key Laboratory of Shale Oil and Gas Enrichment Mechanisms and Effective Development, Sinopec Petroleum Exploration and Production Research Institute (Grant. G5800-20-ZS-KFGY004), the Natural Science Foundation of China (Grant No. 42172140), and the Science Foundation for Distinguished Young Scholars of China University of Petroleum - Beijing (No. 2462020QNXZ004).

References

1. Zhu, R.; Zou, C.; Wu, S.; Yang, Z.; Mao, Z.; Yang, H.; Fan, C.; Hui, X.; Cui, J.; Su, L.; Wang, H. Mechanism for generation and accumulation of continental tight oil in China. *Petroleum and Natural Gas Geology* **2019**, 40, (06), 1168-1184.
2. Zhao, W.; Zhu, R.; Hu, S.; Hou, L.; Wu, S. Accumulation contribution differences between lacustrine organic-rich shales and mudstones and their significance in shale oil evaluation. Petroleum Exploration and Development 2020, 47, (6), 1079-1089.
3. Desmastes, D.; Grosheny, D.; Beaudoin, B.; Gardin S.; Gauthier, L. F. High resolution stratigraphic record constrained by volcanic ash beds at the Cenomanian—turonian boundary in the Western Interior. Basin, USA. *Cretaceous Research* **2007,** 28, (4), 561–582.
4. Liu, Q.; Li, P.; Jin, Z; Sun, Y.; Hu, G.; Zhu, D.; Huang, Z.; Liang, X.; Zhang, R.; Liu, J. 2022. Organic-rich formation and hydrocarbon enrichment of lacustrine shale strata: A case study of Chang 7 Member. *Science China Earth Sciences* **2022**, 65, (1), 118–138.
5. Liang, X.; Jin, Z.; Liu, Q.; Shpilman, A.; Li, P.; Morozov, V.; Uspensky, B. Influence of volcanic ash on the formation of organic-rich shale—an example from the Mesozoic Bazhenov Formation in the West Siberian Basin. *Petroleum and Natural Gas Geology* **2021**, 42, (01), 201-211.
6. Li, Y.; Xu, X.; Zhang, J.; Chen, S.; Bai, J.; Liu, W.; Wang, Q. Hybrid Sedimentary Conditions of Organic - Rich Shales in Faulted Lacustrine Basin during Volcanic Eruption Episode：A Case Study of Shahezi Formation (K_1sh Fm.), Lishu Faulted Depression, South Songliao Basin. *Earth Science* **2022** 47, (5), 1728-1747.
7. Wang, C.; Wang, Q.; Chen, G.; He, L.; Xu, Y.; Chen, L.; Chen D. Petrographic and geochemical characteristics of the lacustrine black shales from the upper Triassic Yanchang formation of the Ordos basin, China: implications for the organic matter accumulation. *Marine and Petroleum Geology* **2017**, 86, 52–65.
8. Yang, S.; Hu, W.; Wang, X.; Jiang B.; Yao, S.; Sun, F.; Huang, Z.; Zhu F. Duration, evolution, and implications of volcanic activity across the Ordovician–Silurian transition in the Lower Yangtze region, South China. *Earth and Planetary Science Letters* **2019**, 518, 13–25.
9. Tian, H.; Fan, M.; Victor, V.; Chamberlain, K.; Waite, L.; Stern, J. R.; Loocke, M. Rapid early Permian tectonic reorganization of Laurentia's plate margins: Evidence from volcanic tuffs in the Permian Basin, USA. *Gondwana Research* **2022**, 111, 76-94.
10. Lowe, J. D. Tephrochronology and its application: A review. *Quaternary Geochronology*, **2011**, 6, (2), 107-153.
11. Tomaru, H.; Lu, Z.; Fehn, U.; Muramatsu, Y. Origin of hydrocarbons in the Green Tuff region of Japan: ^{129}I results from oil field brines and hot springs in the Akita and Niigata Basins. *Chemical Geology* **2009**, 264, 221-231.
12. Zhang, G.; Zou, C.; Zhu, R.; Yuan, X.; Zhao, X. Petroleum geology and exploration for volcanic reservoirs in the sedimentary basins of China. *Strategic Study of CAE* **2010**, 12, (5), 30–38.
13. Stinco, L.; Barredo, S. Geomechanics and electrofacies characterization of the Los Molles Formation (lower to Middle Jurassic), Neuquén Basin. *Journal of South American Earth Sciences* **2021**, 110.
14. Zhang, L.; Li, J.; Song, Y.; Chen, S.; Lu, J.; Guo, J.; Zeng, Y.; Cui, H. Gas accumulation characteristics and exploration potential of the Carboniferous volcanic rocks in Junggar Basin. *China Petroleum Exploration* **2021**, 26, (6), 141-151.
15. Wang, G.; Li, D.; Liu, L.; Dou, Y.; Zheng, Q. Production Analysis and Influencing Factors of Igneous Reservoir in Northwest Margin of Junggar Basin. *Bulletin of science and technology* **2021**, 37, (03), 9-15+21.
16. Wang, J.; Liu, C.; Li, H.; Wu, T.; Wu, J. Geochronology，Potential Source and Regional Implications of Tuff Intervals in Chang-7 Member of Yanchang Formation, South of Ordos Basin. *Acta Sedimentologica Sinica* **2017**, 35, (04), 691-704.
17. Chen, X.; Li, J.; Liang, H.; Luo, Q.; Fan, T.; He, R.; Feng, Y. Hydrocarbon Accumulation Elements Analysis of Tiaohu Tuff Reservoir of Middle Permian, Santanghu Basin. *Xinjiang Petroleum geology* **2014**, 35, (4), 386-390.
18. Pan, Y.; Huang, Z.; Guo, X.; Li, T.; Fan, T.; Xu, X. Analysis of accumulation conditions of lacustrine organic-rich shale oil affected by volcanic ash：a case study of the Lucaogou Formation in the Tiaohu-Malang sag ，Santanghu basin. *Acta Geologica Sinica*, **2022**,96, (3),1053-1068.
19. Wang, J.; Yuan, B.; Liu, J.; Li, Y.; Li, E.; Ma, C.; Zhang, B. Genesis and pore development characteristics of Permian Lucaogou migmatites, Jimsar Sag, Junggar Basin. *Petroleum Geology & Experiment* **2022**, 44, (03), 413-424.
20. Liu, X.; Jiang, Z.; Yuan, X.; Chen, C.; Wang, C. Influence of the Cretaceous fine-grained volcanic materials on shale oil/gas, Luanping Basin. *Oil & Gas Geology* **2022**, 43, (02), 390-406.
21. Zhao, H.; Huang, W.; Wang, C.; Di, Y.; Qi, J.; Xiao, Y.; Liu, J. Micropores from devitrification in volcanic rocks and their contribution to reservoirs. *Oil & Gas Geology* **2009**, 30, (01), 47-52+58.

22. Schembre, J. M.; Tang, G.; Kovscek, A.R. Wettability alteration and oil recovery by water imbibition at elevated temperatures. *Journal of Petroleum Science and Engineering* **2006**, 52, 131-148.
22. Lv, P.; Li, M.; Yang, Z.; Lin, M.; Dong, C.; Peng, B. Review of the Influencing Factors of Reservoir Wettability. *Science Technology and Engineering* **2015**, 15, (25), 88-94.
23. Gao, Z.; Hu, Q. Initial water saturation and imbibition fluid affect spontaneous imbibition into Barnett shale samples. *Journal of Natural Gas Science and Engineering* **2016**, 34, 541-551.
24. Zhou, D.; Li, M.; Shi, Y.; Zou, Y.; Liu, S. Sensitivity Analysis of Imbibition Stability Time in Tight Sandstone Reservoir. *Special Oil and Gas Reservoirs* **2018**, 25, (02), 125-129.
25. Ye, H.; Ning, Z.; Wang, Q.; Cheng, Z.; Huang, L.; Mu, D. Spontaneous imbibition experiment and wettability of shale reservoir. *Fault-Block Oil & Gas Field* **2019**, 26, (01), 84-87.
26. Zhang, Z.; Feng, J.; Cai, J.; Chen, K.; Meng, Q. Driving Force for Spontaneous Imbibition Under
27. Different Boundary Conditions. *Chinese Journal of Computational Physics* **2021**, 38, (05), 513-520.
28. Macquaker, J.; Davies, S. Lithofacies Variability in Fine-Grained Mixed Clastic Carbonate Successions: Implications for Identifying Shale-Gas Reservoir. *AAPG* **2008**.
29. Yang, W.; Wang, Q.; Song, Y.; Jiang, Z.; Meng, W., Liu, G.; Zhang, B. New scaling model of the spontaneous imbibition behavior of tuffaceous shale: Constraints from the tuff-hosted and organic matter-covered pore system. *Journal of Natural Gas Science and Engineering*, **2020**, 81, 103389.
30. Liu, S.; Yao, M.; Feng, Y.; Fan, T. Influencing Factor Analysis of Devitrification Pore and Its Relationship with Hydrocarbon in Tiaohu Formation of Malang Depression. *Special Oil and Gas Reservoir*s **2018**, 25, (01), 16-19.
31. Fu, J.; Luo, S.; Niu, X.; Lu, Q.; Xu, L.; Feng, S.; Li, S.; Sedimentary Characteristics of Channel Type Gravity Flow of the Member 7of Yanchang Formation in the Longdong Area, Ordos Basin. *Bulletin of Mineralogy, Petrology and Geochemistry* **2015**, 34, (01), 29-37+1.
32. Li, D. Return to petroleum geology of Ordos Basin. *Petroleum Exploration and Development*, **2004**, (06), 1-7.
33. Tian, Y.; Zhong, J.; Wang, S.; Tao, H.; Liu, S.; Li, Y.; Sun, N.; Shao, Z.; Ni, L.; Mao, C.; Ge, Y.; Chen, B.; Qu, J.; Wang, G. Seismites and their geological significances of the Triassic Yanchang Formation in Fuxian exploration area, Ordos Basin. *Journal of Palaeogeography* 2015, 17, (04), 541-552.
34. Zhang, J. Tectonic evolution of Ordos Basin and its oil and gas potential. *Oil & Gas Geology* **1982**, (04), 304-315.
35. Qiu, X.; Liu, C.; Mao, G.; Deng, Y.; Wang, F.; Wang, J. Major, trace and platinum-group element geochemistry of the upper Triassic nonmarine hot shales in the Ordos basin, Central China. *Applied Geochemistry* **2015a**, 53, 42–52.
36. Qiu, X.; Liu, C.; Wang, F.; Deng, Y.; Mao, G. Trace and rare earth element geochemistry of the Upper Triassic mudstones in the southern Ordos Basin, Central China. *Geological Journal* **2015b**, 50, (4), 399–413.
37. Yao, J.; Deng, X.; Zhao, Y.; Han, T.; Chu, M.; Pang, J. Characteristics of tight oil in Triassic Yanchang Formation, Ordos Basin. *Petroleum Exploration and Development* **2013**, 40, (02), 150-158.
38. Fu, J.; Li, S.; Niu, X.; Deng, X.; Zhou, X. Geological characteristics and exploration of shale oil in Chang 7 Member of Triassic Yanchang Formation, Ordos Basin, NW China. *Petroleum Exploration and Development* **2020**, 47, (05), 870-883.
39. Fan, B.; Jin, Y.; Shi, L.; Li, Y.; Chen, W. Shale oil exploration potential in central Ordos Basin:A case study of Chang 7 lacustrine shale. *Oil & Gas Geology* **2021**, 42, (05), 1078-1088.
40. Fan, B.; Shi, L.; Yang, J.; Su, S.; Ma, R.; Yuan, Y.; Zeng, C. Sedimentary environment of lacustrine organic matter in the central Ordos Basin. *Oil & Gas Geology* **2022**, 43, (03), 648-657.
41. Tang, X.; Zhang, J.; Jin, Z.; Xiong, J.; Lin, L.; Yu, Y.; Han, S. Experimental investigation of thermal maturation on shale reservoir properties from hydrous pyrolysis of Chang 7 shale, Ordos Basin. *Marine and Petroleum Geology* **2015**, 64, 165-172.
42. Dou, W.; Liu, L.; Wu, K.; Xu, Z.; Liu, X.; Feng, X. Diagenetic heterogeneity, pore throats characteristic and their effects on reservoir quality of the Upper Triassic tight sandstones of Yanchang Formation in Ordos Basin, China. *Marine and Petroleum Geology* **2018**, 98, 243-257.
43. Yang, Y.; Song, C.; He, S. Jurassic tectonostratigraphic evolution of the Junggar basin, NW China: A record of Mesozoic intraplate deformation in Central Asia. *Tectonics* **2015**, 34, (1), 86–115.
44. Wu, K.; Zha, M.; Wang, X.; Qu, J.; Chen, X. Further Researches on the Tectonic Evolution and Dynamic Setting of the Junggar Basin. *Acta Geoscientica Sinica* **2005**, (03), 217-222.
45. Wu, Q. An overview of the developmental stages, tectonic units and local tectonic genesis of the Junggar Basin. *Xinjiang Petroleum geology* **1986**, (01), 29-37.
46. Yang, H.; Chen, L.; Kong, Y. A Novel Classification of Structural Units in Junggar Basin. *Xinjiang Petroleum geology* **2004**, (06), 686-688.

47. Wang, X. Stratigraphic framework and sedimentary evolution of the Permian-Jurassic in the surrounding area of the Bogda Mountains. *China University of Petroleum (East China)* **2017**.
48. Lou, J.; Tian, J.; Ma, J.; Yan, J.; Liang, Y.; Hu, Z. Sedimentary environment and organic matter enrichment mechanism of Permian Lucaogou Formation in Jiye-1 well area, Jimsar Sag. *Lithologic Reservoirs*, 2022, 34, (5), 73-85.
49. Gao, F.; Wang, C.; Song, Y.; Chen, Z.; Liu, Q. Li, Z.; Jiang, Z.; Zhang, X. Ar-ion polishing FE—SEM analysis of organic maceral identification. *Petroleum Geology and Experiment* **2021**, 43, (02), 360-367.
50. Li, C.; Li, Y.; Chen, X.; Liu, Z.; Li, P.; Wang, Y. Pore characterization of the Permian shale in the Wuhu area using FE-SEM technique. *Journal of Chinese Electron Microscopy Society* **2020**,39, (02), 151-157.
51. Chen, T.; Xie, Q. From optical microscopy to electron microscopy: Nanogeoscience. *Journal of Hefei University of Technology* **2005**, (09), 126-1129.
52. Gu, L.; Li, J. The Focused Ion Beam (FIB) Technology and its Applications for Earth and Planetary Sciences. *Bulletin of Mineralogy, Petrology and Geochemistry* **2020**, 39, (06), 1119-1140+1065-1066.
53. Wang, D.; Bltler, R.; Zhang, J.; Seright, R. Wettability survey in Bakken shale with surfactant-formulation imbibition. *SPE Reservoir Evaluation & Engineering* **2012**, 15, (06), 695-705.
54. Gao, Z.; Liang, Z.; Jiang, Z.; Xiong, S.; Duan, L.; Yang, B.; Zheng, G. A method and equipment for evaluating the wettability of shale reservoirs. *China National Intellectual Property Office* **2022.**
55. Land L. S. Failure to Precipitate Dolomite at 25°C from Dilute Solution Despite 1000-Fold Oversaturation After 32 Years. *Aquatic Geochemistry* **1998,** 4, (3-4), 361-368.
56. Huang, C.; Yuan, J.; Cao, Z.; Zhang, S.; Wang, Y.; She, M.; Mi, H. Simulation experiment for ankerite dissolution in clastic reservoir of saline lacustrine basin. *Petroleum Geology & Experiment* **2014**, 36, (5), 650-655.
57. Mchenry L. J. Element mobility during zeolitic and argillical teration of volcanic ash in a closed-basin lacustrine environment: Case study Olduvai Gorge, Tanzania. *Chemical Geology* **2009**, 265, 540-552.
58. Kirov, G.; Šamajova, E.; Nedialkov, R.; Stanimirova, T. Alteration processes and products of acid pyroclastic rocks in Bulgaria and Slovakia. *Clay Minerals* **2011**, 46, (2), 279-294.
59. Ma, J.; Hung, Z.; Liu, Z.; Chen, C.; Gao, X. Tight reservoir characteristics of sedimentary organic matter-bearing tuff in Tiaohu Formation of Santanghu Basin. *Earth Science Frontiers* **2015**, 22, (6), 185-196.
60. Marquez, X. M.; Mountjoy, E. W. Microfractures due to overpressures caused by thermal cracking in well-sealed Upper Devonian reservoirs, deep Alberta Basin. *AAPG Bulletin* **1996**，80, (4), 570-588.
61. Wang, R.; Sun, W. A study on micro cracks in super low permeability sandstone reservoir of the Upper Triassic Yanchang Formation in the Ordos Basin. *Geological Review*, **2009**, 55, (3), 444-448.
62. Nan, J.; Wang, S.; Yao, W.; Lu, Y. Micro-fractures in extra low permeability reservoir of Yanchang Formation in Ordos Basin. *Lithological Reservoirs* **2007**, 19, (4), 40-44.
63. Camp, W. K. Strategies for Identifying Organic Matter Types in SEM. *American Association of Petroleum Geologists Search and Discovery Article* **2017**, 70233.
64. Wood, J. M.; Sanei, H.; Curtis, M. E.; Clarkson, C. R. Solid bitumen as a determinant of reservoir quality in an unconventional tight gas siltstone play. *International Journal of Coal Geology* **2015**, 150–151, 287–295.
65. Yao, Y.; Liu, D. Microscopic characteristics of microfractures in coals：An investigation into permeability of coal. *Procedia Earth and Planetary Science* **2009**, 1, (1), 903-910.
66. Wang, J.; Bao, Z.; Chen, M.; Sun, F.; Liu, R.; Zhao, M.; Sun, Q. Differention of sandstones'tuff fillings and its effect on porosity—An Example from the Paleozoic Sandstones in Northwestern Ordos. *Chinese Journal of Geology* **2005**, (03), 429-438.
67. Zhu, G.; Zhang, J.; Yao, G.; Li, Y.; Wang, X.; Yu, C. Sedimentary Volcanic Dust Tuff, An Important Kind of Rock Storing Hydrocarbon Resources: Discussion on the Lithology of Middle Permian Lucaogou Oil-bearing Rocks in the North of Xinjiang. *Marine Origin Petroleum Geology*, **2014**, 19, (01), 1-7.
68. Marshall, R.R. Devitrification of natural glass. *Geological Society of America Bulletin* **1961**. 72, 1493–1520.
69. Zheng, H.; Sun, X.; Wang, J.; Zhu, D.; Zhang, X. Devitrification pores and their contribution to volcanic reservoirs: a case study in the Hailar Basin, NE China. *Marine and Petroleum Geology* **2018b**, 98, 718–732.
70. Zhu, S.; Zhu, X.; Liu Y.; Chen X.; Wang, J.; Wang, X.; Ma A. Petrological and Geochemical Features of Dolomitic Rocks in the Lower Permian Fengcheng Formation in Wuerhe—Xiazijie Area，Junggar Basin. *Geological Review* **2014**, 60, (05), 1113-1122.
71. Qiu, L.; Jiang, Z.; Chen, W.; Li, X.; Xiong Z. A New Type of Secondary Porosity—Quartz Dissolution Porosity. *Acta Sedimentologica Sinica* **2002**, (04), 621-627.
72. Nickel, E. H.; Grice, J. D. The IMA commission on new minerals and mineral names: Procedures and guidelines on mineral nomenclature. *The Canadian Mineralogist* **1998**, 36, 10-20.
73. Fu, Q.; Sun, X.; Liu, Y. Geologic Significance and Re-establishment of Basin Character in Late Triassic of Ordos Basin. *Journal of Tongji University* **2009**, 37, (11), 1537-1540.

 doi:10.20944/preprints202312.0616.v1